RESEARCH

QbD-driven RP-HPLC method for novel chemo-herbal combination, in-silico, force degradation studies, and characterization of dual drug-loaded polymeric and lipidic nanocarriers

Ankaj Kumar[1], Sandeep Jat[2], Pramod Kumar[2] and Arvind Gulbake[1*]

Abstract

Background In cancer therapies, chemo-herbal combinations are receiving increased attention. A multiple tyrosine kinase inhibitor, lenvatinib (LTB) is beneficial in treating thyroid, lung, endometrial, and liver cancers. An isoflavone called biochanin A (BCA) is well known for its diverse biological properties that have been studied to potentiate the anti-cancer potential and lower the normal cell toxicities of other therapeutics. LTB and BCA can be combined for cancer treatment and may increase their therapeutic potential at lower doses. In brief, the quality by design (QbD)-driven RP-HPLC method was developed, validated, and utilized for applications employing the study of forced degradants and the successful development of LTB and BCA co-loaded nanocarriers.

Results The RP-HPLC method employed Box–Behnken design with peak resolution 6.70 ± 0.006, tailing factor 1.06 ± 0.05 for BCA and 1.17 ± 0.021 for LTB, and theoretical plates number > 2000. RP-HPLC applications utilized the investigation of a total of 41.17% and 70.58% degradants for LTB and BCA in contrast to in-silico predicted studies using Zeneth software. The poly (lactic-*co*-glycolic acid) nanoparticles (PLGA NPs) were formed with particle size 185.3 ± 12.3 nm, zeta potential -13.3 ± 0.35 mV, and percentage entrapment efficiency (%EE) for the LTB and BCA $53.64 \pm 4.81\%$ and $61.29 \pm 4.67\%$, respectively. However, the developed Cubosomes (CBs) exhibited 182.4 ± 16.3 nm aerodynamic particle size, -10.8 ± 0.39 mV zeta potential, and % EE for LTB and BCA $55.62 \pm 7.73\%$ and $72.88 \pm 5.52\%$, respectively. The percentage drug loading (%DL) of LTB and BCA from PLGA NPs was found to be $3.7 \pm 0.46\%$ and $4.63 \pm 0.48\%$, whereas CBs exhibited higher % DL for BCA ($5.42 \pm 1.10\%$) and LTB ($4.43 \pm 0.77\%$).

Conclusion The RP-HPLC method was developed and validated according to ICH and USP guidelines. In-vitro and in-silico forced degradation studies are evident to quantify the type of degradant and its exact mechanism of degradation. In-silico toxicity assessment for LTB, BCA, and their degradants explains the necessity of conducting degradation studies during drug development. Finally, the applications of the developed RP-HPLC method explain the usefulness of analytical methods in the development of chemo-herbal drug nanocarriers (polymeric and lipidic).

*Correspondence:
Arvind Gulbake
arvind@niperguwahati.in
Full list of author information is available at the end of the article

Highlights

- The RP-HPLC method was developed for a multiple tyrosine kinase inhibitor (MTKI), lenvatinib (LTB), and an isoflavone called biochanin A (BCA), employing Box–Behnken design (BBD).
- A total of 41.17% and 70.58% degradants were quantified through experimental investigation (RP-HPLC and HRMS) for LTB and BCA in contrast to in silico predicted degradants.
- In-silico toxicity assessment for LTB, BCA, and their degradants explains the necessity of conducting degradation studies during drug development.
- Finally, the applications of the developed RP-HPLC method for the development of chemo-herbal drug nanocarriers (polymeric and lipidic) were studied.

Graphical abstract
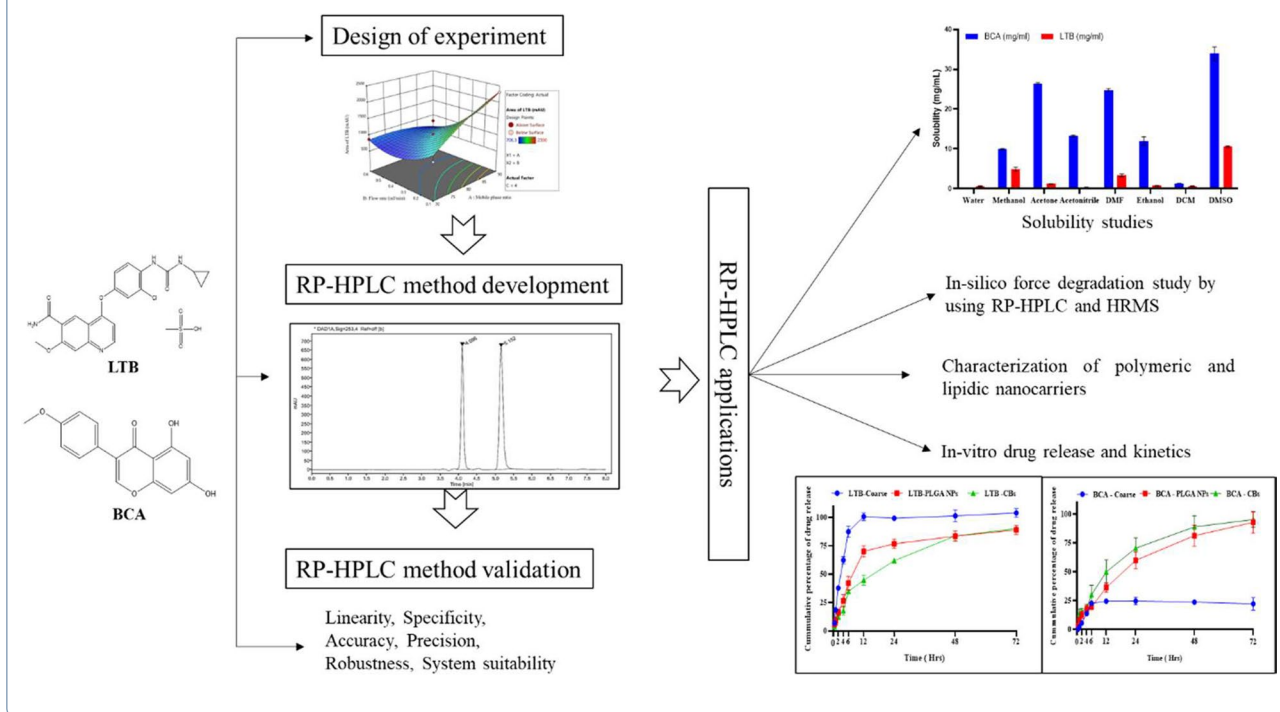
Background

In the field of cancer therapies, the chemo-herbal combination has received increased attention [1]. A combination can change signaling pathways, which may have a synergistic effect and may help to overcome resistance mechanisms [2, 3]. The chemo-herbal combination can be investigated using the appropriate polymeric and lipidic drug carriers [4]. Validated analytical methods are necessary to measure each chemo or herbal drug with good sensitivity accurately.

Lenvatinib (LTB), a multiple receptor tyrosine kinase inhibitor, was initially approved by the Food and Drug Administration (FDA) in February 2015 for the treatment

of thyroid cancer. It was later approved as part of combination therapy for the treatment of advanced renal cell carcinoma [5]. LTB alone or combined with other therapeutics are under preclinical or clinical trials for lung, liver, and endometrial cancer [6–8]. The chemical structure of LTB is depicted in Fig. 1A. The underlying mechanism of LTB involves specificity or targetability toward tumor and vascular endothelial cell kinase receptors (Vascular endothelial growth factor receptors, epidermal growth factor receptors, mitogen-activated protein kinase, colony-stimulating factor-1 receptors, anaplastic lymphoma kinase, FMS- related tyrosine kinase-3, platelet-derived growth factor receptors) to block the
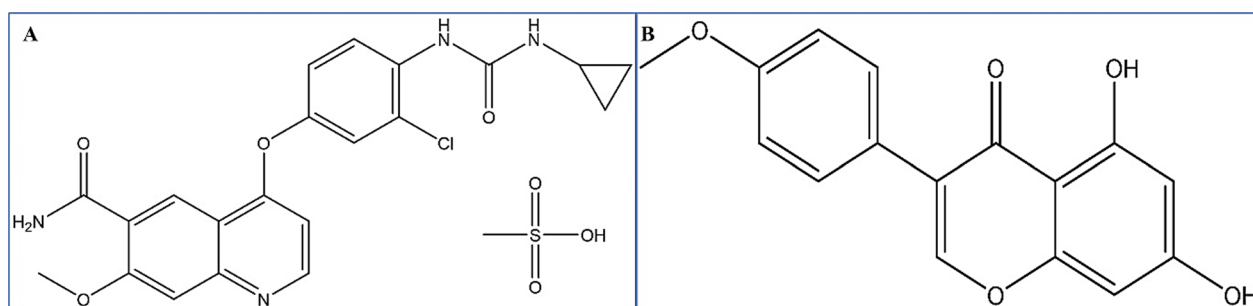
Fig. 1 Chemical structure of **A** lenvatinib mesylate and **B** biochanin A

signaling transduction pathways that participate in the progression of cancer [6, 8]. However, the side effects, toxicity toward normal cells, and lower bioavailability of LTB are the hurdles that require a drug combination to strengthen the biological performance in lower doses. It also finds the use of a drug carriers to deliver the drug at the specific disease site without harming normal cells [9–12].

An isoflavone biochanin A (BCA) is well known to potentiate the anti-cancer effects of chemotherapeutics [13]. The effectual therapies were established by a combination of BCA with sorafenib [14], doxorubicin [15], 5-fluorouracil [16], and BRAF inhibitor SB590885 [17].

BCA is an isoflavone extracted from the leaves and stems of different varieties of red clover, chickpea, and soy plants. Generally, the plant varieties that contain BCA are Cicer arietinum, Trifolium pratense, Cassia fistula, Dalbergia paniculata, Arachis hypogaea, Medicago sativa, and Astragalus membranaceus [18]. The chemical structure of BCA is depicted in Fig. 1B. BCA has various biological activities, including anti-cancer, anti-inflammatory, antioxidant, anti-microbial, and hepatoprotective [19]. BCA's anti-inflammatory and anti-cancer role makes it an ideal therapeutic agent in cancer therapies [20]. In general, it restricts DNA replication in the S phase, decreases the B-cell lymphoma-2 production, increases the Bax-2 protein expression, and inhibits the proinflammatory cytokines in cancer, thus producing an anti-cancer effect [21, 22]. BCA restricts the nuclear transcription factor (NF-kB) by inhibiting several proteins, mainly serine/threonine kinase activity [23]. The development of resistance through P-glycoprotein can also be inhibited through BCA, as reported by Zhang et al. [24]. In addition, BCA stimulates anti-COPD/asthma bioactivities and prevents lung injury by regulating toll-like receptor-4/NF-κB and peroxisome proliferator-activated receptors -γ pathway [25–27]. The poor aqueous solubility of BCA restricts such anti-cancer potential and requires a suitable drug carrier to prevent such progression of cancer [28].

The combination of drug development in terms of desired products requires suitable analytical methods for their successful investigation. It became necessary to study the degradants of each drug that can affect the therapeutic potential. The formed degradants can also be toxic and thus require a brief understanding of such to take necessary precautions during their development phases.

The study includes developing and validating the RP-HPLC method for simultaneous estimation of LTB and BCA. Force degradation studies were employed to check the mechanism underlying the degradants, and in-silico prediction models have also been used to study the prediction of degradants and toxicity assessment. The degradants of LTB and BCA were identified utilizing RP-HPLC and HRMS. Finally, the developed HPLC method was utilized to access quantification applications in the development of dual drugs-embedded polymeric and lipidic nanocarriers.

Materials

All the chemicals purchased were of analytical grades with > 99% purity. Biochanin A, lenvatinib, and lipid, glyceryl monooleate (GMO) were purchased from TCI Co., Ltd (Hyderabad, India). The PLGA and cellulose dialysis tube of 12KDa molecular weight were purchased from Sigma-Aldrich (St. Louis, MO, USA).

Methods

Selection of wavelength

The UV–Vis spectrophotometer was used to check the wavelength with maximum absorbance at the 200–800 nm range. Briefly, the primary stock (1000 µg/mL) solution was prepared by adding 5 mg/5 mL LTB in methanol and BCA in acetonitrile (ACN) separately. The solvent selection was made based on the higher solubility of the drug. The different secondary stock solution (100 µg/mL) was prepared by taking 100 µl of each drug solution and diluting up to make 1 mL volume using ACN. The working standard of both the drugs 10 µg/mL was made

Kumar *et al. Future Journal of Pharmaceutical Sciences* (2023) 9:110

Page 4 of 25

separately by the addition of 100 µl secondary stock solutions of LTB and BCA in 900 µl ACN as diluent. An aliquot of 10 µg/mL concentration was taken in quartz cell cuvette and scanned to detect wavelength with maximum absorption (λmax) in the range 200–800 nm using ACN as blank in a double beam UV–Vis spectrophotometer (UV-2600, Shimadzu, Japan). Finally, the merged overlay of the UV absorption spectrum for LTB and BCA was obtained to determine both drugs' isosbestic wavelengths with maximum absorption [29].

Instrumentation

The high-performance RP-HPLC (Agilent 1260 Infinity II) instrument is equipped with an autosampler, quaternary pump, and PDA detector (1260 DAD WR). The Agilent Open lab application (Version 7.2.8) was used to control the instrumental and process parameters. The instrument is also equipped with an adjustable temperature oven. The stationary phase (YMC-Pack Pro C18 150×4.6 mm L.D. S-5 µm,12 nm) was taken for the study. The RP-HPLC method development for drugs (LTB and BCA) was conducted by taking ACN and acidified water (0.1% formic acid added to water pH 4). The ratio optimization of the mobile phase was assessed by analysis of dependent variables (peak resolution, area of LTB and BCA, theoretical plate numbers, and tailing factor).

Development of RP-HPLC method using design of experiment

Optimization is the crucial process that drives critical process parameters (CPP) and critical analytical attributes (CAAs) to achieve a quality-targeted method profile (QTMP). The QTMP considered for the RP-HPLC method was the area of LTB, area of BCA, peak resolution, and tailing factor for LTB and BCA. To achieve QTMP from the proposed developed HPLC method, independent variables (solvent and process-based) were considered. The crucial independent factors were the mobile phase ratio, flow rate, and pH of the aqueous phase. The selection of such was done using manual trial and literature. The RP-HPLC method was developed by varying independent variables to get optimum dependent variables according to ICH (Q2A) guidelines. The BBD employing a design expert software was used to develop the RP-HPLC method and assess each factor's effect on dependent variables [30]. A 2^3 level BBD design was selected, having a total of 17 runs varying -1 and $+1$ level values for each independent variable. The narrow range of -1 and $+1$ values was selected to see the critical effect that was selected based on manual trials and literature. The data from each run were fitted for different models and evaluated for significant values employing an analysis of variance tables. The coded equation was generated for each response to correlate the effect of each factor on the

dependent variable. The validation of the design model was assessed from the p-value, R^2 values (predicted and adjusted), and normal distribution plots. The response surface graphs were plotted to visualize the effect of each factor and combination of factors on each response. The overlay plots were plotted to see the optimum factors required to generate the desired responses. The 10 µg/mL concentration of LTB and BCA was selected owing to their good system suitability parameters according to ICH guidelines to optimize the independent variable and to develop the RP-HPLC method.

Assay validation

The simultaneous detection, quantification, and validation were done through the RP-HPLC method per the International Council for Harmonization (ICH) of Technical Requirements for Human Use Guideline. The method was validated concerning specificity, linearity, range, precision, accuracy, sensitivity, and robustness. The system suitability study was followed as per United States Pharmacopoeia (USP) guidelines [29, 31, 32]. The methodology adopted to validate the developed RP-HPLC method is discussed in the supplementary section.

Applications of RP-HPLC in degradation studies
In-silico degradation profiling and toxicity assessment of BCA and LTB

In-silico degradation studies provide insight into a prediction of various degradants and their toxicity assessment to explain the importance of conducting such investigations. The different stress conditions as hydrolytic (acidic, basic, and neutral pH levels) and oxidative stress were used to determine the degradation behavior of BCA and LTB. An in-silico analysis aids in predicting the likelihood of study results. The anticipated investigation was employed by Zeneth 9.0 software to analyze the drug molecules under various stress conditions to identify the types of degradants present, their molecular weight, structural makeup, and types of degradation. The software was configured to forecast the various degradants based on the hydrolytic conditions (acidic, basic, and neutral) and oxidative stress conditions [33]. The oxidative hydrolytic degradation pathway for LTB mesylate predicts a total of 18 degradants as explained in Table 1 for their structure, molecular formula, average mass, conditions, and types of degradation. To support the in-silico forced degradation study, a stress study using RP-HPLC and HRMS was conducted. Briefly, the stock solutions (1000 µg/mL) of BCA and LTB were prepared and exposed to 0.1N HCL, 0.1N NaOH, and neutral hydrolytic conditions at 80 °C for 2 h. An addition of stock solution in a hydrolytic medium was assumed to reduce the drug concentration

Table 1 In-silico prediction profile of lenvatinib mesylate degradation at different stress conditions by Zeneth software
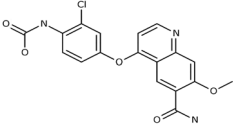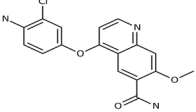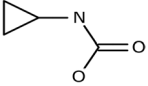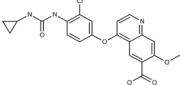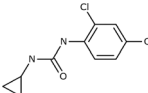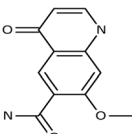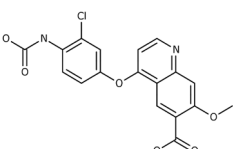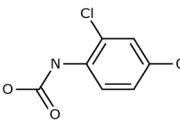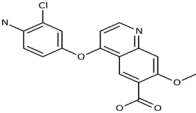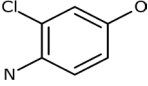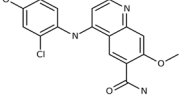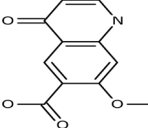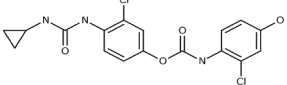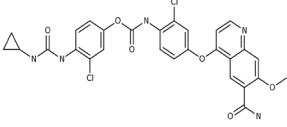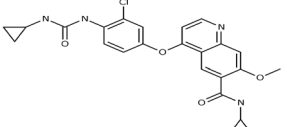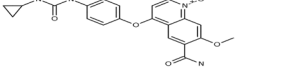
Degradant	Chemical structure	Molecular formula	Mass (*m/z*)	Trigger conditions	Types
Acidic hydrolytic conditions					
LD1		C_3H_7N	57.09	Water; pH	Hydrolysis of urea
LD2		$C_{18}H_{14}ClN_3O_5$	387.77	Water; pH	Hydrolysis of urea
LD3		$C_{17}H_{14}ClN_3O_3$	343.76	Water; pH	Hydrolysis of urea
LD4		$C_4H_7NO_2$	101.1	Water; pH	Hydrolysis of urea
LD5		$C_{21}H_{18}ClN_3O_5$	427.84	Water; pH	Hydrolysis of amide
LD6		$C_{10}H_{11}ClN_2O_2$	226.66	Water; pH	Hydrolysis of 4-heterosubstituted pyridine or related compound
LD7		$C_{11}H_{10}N_2O_3$	218.21	Water; pH	Hydrolysis of 4-heterosubstituted pyridine or related compound
LD8		$C_{18}H_{13}ClN_2O_6$	388.76	Water; pH	Hydrolysis of amide
LD9		$C_7H_6ClNO_3$	187.58	Water; pH	Hydrolysis of 4-heterosubstituted pyridine or related compound
LD10		$C_{17}H_{13}ClN_2O_4$	344.75	Water; pH	Hydrolysis of amide
LD11		C_6H_6ClNO	143.57	Water; pH	Hydrolysis of 4-heterosubstituted pyridine or related compound
LD12		$C_{17}H_{14}ClN_3O_3$	343.76	pH	Intramolecular nucleophilic aromatic substitution of 4-heterosubstituted pyridine or related compound
LD13		$C_{11}H_9NO_4$	219.19	Water; pH	Hydrolysis of 4-heterosubstituted pyridine or related compound

Kumar *et al. Future Journal of Pharmaceutical Sciences*   (2023) 9:110

Page 6 of 25

Table 1 (continued)

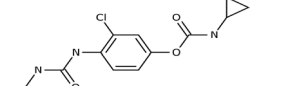| Degradant	Chemical structure	Molecular formula	Mass (*m/z*)	Trigger conditions	Types
LD14		$C_{17}H_{15}Cl_2N_3O_4$	396.23	pH	Transesterification of urea or carbamate ester
LD15		$C_{14}H_{16}ClN_3O_3$	309.75	pH	Transesterification of urea or carbamate ester
LD16		$C_{28}H_{23}Cl_2N_5O_6$	596.42	pH	Transesterification of urea or carbamate ester
Basic hydrolytic conditions					
LD17		$C_{24}H_{23}ClN_4O_4$	466.92	pH	Transamidation with primary aliphatic amine
LD18		$C_{21}H_{19}ClN_4O_5$	442.85	Oxygen or Peroxide; pH	*N*-Oxidation of pyridine-type nitrogen

to 100 µg/mL. After optimized time points, samples were withdrawn and partially adjusted for neutral pH. The withdrawn sample was assumed to have a 10 µg/mL concentration that was analyzed for their stress degradation behavior through RP-HPLC [34].

A total of thirty-four degradants were predicted owing to oxidation and hydrolysis or BCA employing an in-silico degradation study. The degradants were reported as BD1-BD34 for their chemical structure, molecular formula, average mass, and conditions employed for such degradation, as shown in Table 2. Among all such degradants, major degradants as parent ions were studied through RP-HPLC and HRMS.

Chromatographic separation was achieved on a 1290 Infinity II ultra-high-performance liquid chromatography (UHPLC) system (Agilent Technologies, USA) equipped with a ZORBAX SB-C18 column (2.1×100 mm, 1.8 µm), M/s Agilent Technologies. The isocratic mode was used comprised aqueous formic acid and acetonitrile (1:1) with a flow rate of 0.4 mL/min and a loading volume of 22 µl. The electrospray ionization (ESI) source and the Agilent 6545 Accurate Mass Q-TOF/MS system were used to exhibit higher resolution. Briefly, the parameters used were drying gas (N_2) flow rate, 8L/min; temperature, 320 °C; fragmentor voltage, 175; capillary voltage, 3500; and nebulizer gas pressure 35 psi [35].

In-silico toxicity studies

The study involves the in silico toxicity model (Derek EC3 prediction model 2022.2) to predict the toxicity of drug molecules and their degradants. It became essential to know the toxicity of the drug or degradants to take necessary precautions during their development phase. The Derek analysis involves different models as bacterium, hamsters, E. Coli, dogs, guinea pigs, humans, mammals, mice, primates, rats, rabbits, rodents, etc., for skin sensitization and mutagenicity toxicity studies [33].

Application of RP-HPLC method in the development of drug nanocarriers (Polymeric and Lipidic)
Selection of solvent to produce PLGA NPs and CBs

To choose the best solvent throughout the formulation development phase, it is essential to estimate a drug's solubility. Drug in-vitro and in-vivo research, as well as the creation of analytical procedures and drug products, were all aided by the solubility-based solvent screening. The developed RP-HPLC method was used to determine the saturation solubility of LTB and BCA using the shake flask process. Briefly, 1 mg of LTB and BCA was added in 1 mL of different organic solvents (based on applications) till saturation was observed. The samples were kept in an orbital shaker for 24 h at room temperature. After 24 h samples were collected, filtered, diluted, and injected to quantify through RP-HPLC for the concentration of each

Table 2 In-silico prediction profile of Biochanin A (BCA) degradation at different stress conditions by Zeneth software
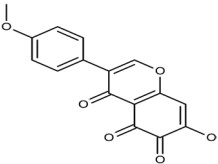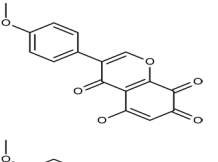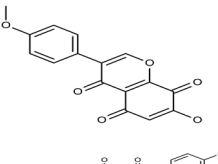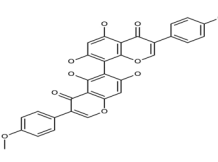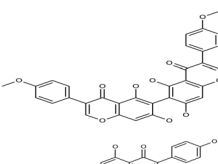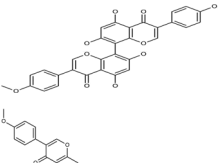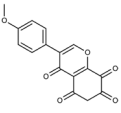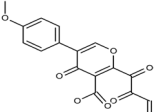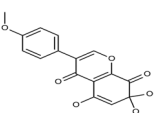
Degradants	Structure	Formula	Average mass (*m/z*)	Condition triggers	Type
BD1		$C_{16}H_{10}O_6$	298.25	Metal; oxygen or peroxide	Oxidation of phenol or aniline to quinone or iminoquinone
BD2		$C_{16}H_{10}O_6$	298.25	Metal; oxygen or peroxide	Oxidation of phenol or aniline to quinone or iminoquinone
BD3		$C_{16}H_{10}O_6$	298.25	Metal; oxygen or peroxide	Oxidation of phenol or aniline to quinone or iminoquinone
BD4		$C_{32}H_{22}O_{10}$	566.51	Metal; oxygen or peroxide	Oxidative coupling of phenols
BD5		$C_{32}H_{22}O_{10}$	566.51	Metal; oxygen or peroxide	Oxidative coupling of phenols
BD6		$C_{32}H_{22}O_{10}$	566.51	Metal; oxygen or peroxide	Oxidative coupling of phenols
BD7		$C_{16}H_{10}O_6$	298.25	None	Tautomerization of enol, enethiol or enamine
BD8		$C_{16}H_{12}O_7$	316.26	Water	Hydration of aldehyde or ketone to geminal diol
BD9		$C_{16}H_{12}O_7$	316.26	Water	Hydration of aldehyde or ketone to geminal diol
BD10		$C_{16}H_{10}O_6$	298.25	None	Tautomerization of enol, enethiol or enamine
BD11		$C_{16}H_{10}O_8$	330.25	Light; oxygen	Oxidative cleavage of alkene

Kumar *et al. Future Journal of Pharmaceutical Sciences*   (2023) 9:110

Page 8 of 25

Table 2 (continued)
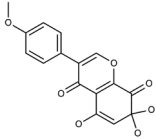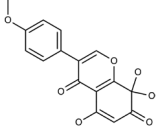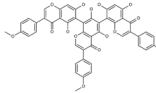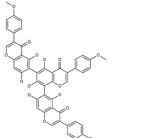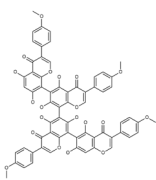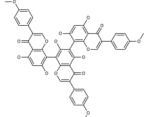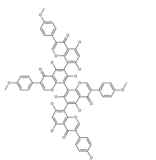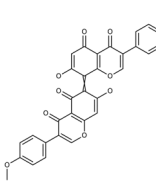
Degradants	Structure	Formula	Average mass (*m/z*)	Condition triggers	Type
BD12		$C_{16}H_{12}O_7$	316.26	Water	Hydration of aldehyde or ketone to geminal diol
BD13		$C_{16}H_{12}O_7$	316.26	Water	Hydration of aldehyde or ketone to geminal diol
BD14		$C_{48}H_{32}O_{15}$	848.76	Metal; oxygen or peroxide	Oxidative coupling of phenols
BD15		$C_{48}H_{32}O_{15}$	848.76	Metal; oxygen or peroxide	Oxidative coupling of phenols
BD16		$C_{64}H_{42}O_{20}$	1131	Metal; oxygen or peroxide	Oxidative coupling of phenols
BD17		$C_{64}H_{42}O_{20}$	1131	Metal; oxygen or peroxide	Oxidative coupling of phenols
BD18		$C_{48}H_{32}O_{15}$	848.76	Metal; oxygen or peroxide	Oxidative coupling of phenols
BD19		$C_{64}H_{42}O_{20}$	1131	Metal; oxygen or peroxide	Oxidative coupling of phenols
BD20		$C_{32}H_{20}O_{10}$	564.5	Oxygen or peroxide	Oxidation of biphenyldiol to biphenyldione

Kumar *et al. Future Journal of Pharmaceutical Sciences*   (2023) 9:110
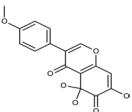
Page 9 of 25

Table 2 (continued)
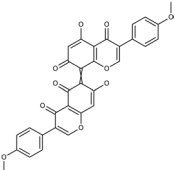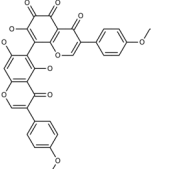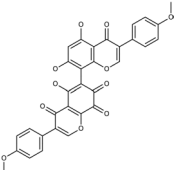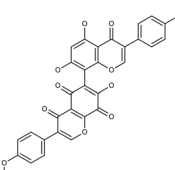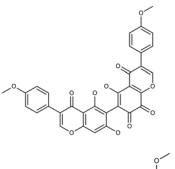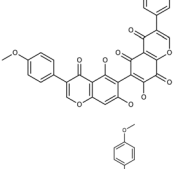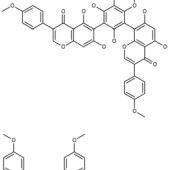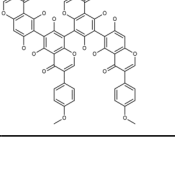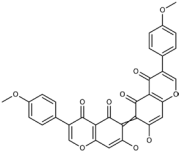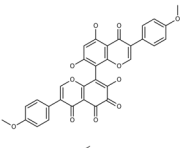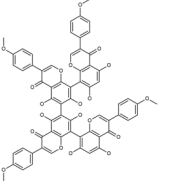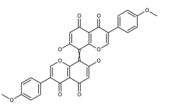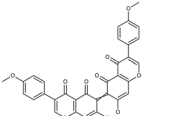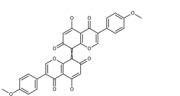
Degradants	Structure	Formula	Average mass (*m/z*)	Condition triggers	Type
BD21		$C_{32}H_{20}O_{10}$	564.5	Oxygen or peroxide	Oxidation of biphenyldiol to biphenyldione
BD22		$C_{32}H_{20}O_{11}$	580.5	Metal; oxygen or peroxide	Oxidation of phenol or aniline to quinone or imino-quinone
BD23		$C_{32}H_{20}O_{11}$	580.5	Metal; oxygen or peroxide	Oxidation of phenol or aniline to quinone or imino-quinone
BD24		$C_{32}H_{20}O_{11}$	580.5	Metal; oxygen or peroxide	Oxidation of phenol or aniline to quinone or imino-quinone
BD25		$C_{32}H_{20}O_{11}$	580.5	Metal; oxygen or peroxide	Oxidation of phenol or aniline to quinone or imino-quinone
BD26		$C_{32}H_{20}O_{11}$	580.5	Metal; oxygen or peroxide	Oxidation of phenol or aniline to quinone or imino-quinone
BD27		$C_{48}H_{32}O_{15}$	848.76	Metal; oxygen or peroxide	Oxidative coupling of phenols
BD28		$C_{64}H_{42}O_{20}$	1131	Metal; oxygen or peroxide	Oxidative coupling of phenols

Kumar *et al. Future Journal of Pharmaceutical Sciences*   (2023) 9:110

Page 10 of 25

Table 2 (continued)

Degradants	Structure	Formula	Average mass (*m/z*)	Condition triggers	Type
BD29		$C_{32}H_{20}O_{10}$	564.5	Oxygen or peroxide	Oxidation of biphenyldiol to biphenyldione
BD30		$C_{32}H_{20}O_{11}$	580.5	Metal; oxygen or peroxide	Oxidation of phenol or aniline to quinone or imino-quinone
BD31		$C_{64}H_{42}O_{20}$	1131	Metal; oxygen or peroxide	Oxidative coupling of phenols
BD32		$C_{32}H_{20}O_{10}$	564.5	Oxygen or peroxide	Oxidation of biphenyldiol to biphenyldione
BD33		$C_{32}H_{20}O_{10}$	564.5	Oxygen or peroxide	Oxidation of biphenyldiol to biphenyldione
BD34		$C_{32}H_{20}O_{10}$	564.5	Oxygen or peroxide	Oxidation of biphenyldiol to biphenyldione

drug utilizing linear regression equations of LTB and BCA [36].

Preparation of polymeric and lipidic nanocarriers
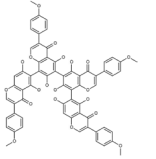The successful production of PLGA NPs was accomplished using the nanoprecipitation technique. In a nutshell, an organic phase with a (4:1) PLGA to drugs ratio was created. As a stabilizer, 1% tween-80 solution was added to the aqueous phase. When the organic phase is added to the aqueous phase, nanoprecipitation starts to happen at 1000 rpm on a magnetic stirrer. By using a rotary evaporator, the organic solvent was removed, and PLGA NPs were thoroughly characterized for their particle size, PDI, and zeta potential [37]. The RP-HPLC was used to quantify the percentage of entrapment efficiency (%EE), percentage of drug loading (%DL), and percentage of LTB and BCA release from PLGA NPs.

The lipidic drug nanocarriers (cubosomes) were generated using the hot melt emulsification technique. Drugs and lipids (GMO) (10:1) were mixed in methanol to give

a lipid phase. The pluronic P-407 (1%) was taken as a stabilizer to form a water-phase system. The bulk cubic phase was produced by mixing the lipid phase with the water phase. The bulk phase was subsequently treated to produce uniformly sized nanoparticles using a high-speed homogenizer (1000 rpm) and probe sonicator (25% amplitude for 10 min) [38]. The CBs were thoroughly characterized using a zeta-sizer for particle size, PDI, and zeta potential.

Characterization of drug nanocarriers
The percentage entrapment efficiency (%EE) of LTB and BCA
After the successful generation of drug nanocarriers, both types of NCs were characterized for a % EE using developed RP-HPLC method. It involves a 10 kDa ultra centrifuge Amicon filter to separate the free drug and NCs with 5000 rpm at room temperature. The direct and indirect methods were used to assess the amount of LTB and BCA entrapped inside the PLGA NPs and CBs. The drugs were quantified using the RP-HPLC method

Kumar *et al. Future Journal of Pharmaceutical Sciences*   (2023) 9:110

Page 11 of 25

and analyzed further from the regression equations. The calculation of %EE was done using Eq. 1 [38, 39].

$$\%EE = \left(\frac{\text{Observed drug concentration}}{\text{Total drug concentration}} \right) \times 100 \quad (1)$$

Percentage drug loading (%DL)

It represents the amount of drug loaded per unit weight of the nanocarriers and shows what proportion of the mass of NCs is attributable to the drug that has been encapsulated. Briefly, the method involves solubilizing the 10 mg of lyophilized nanocarriers using acetonitrile for PLGA NPs and methanol for CBs. The samples were analyzed using RP-HPLC method and calculated for %DL from PLGA NPs and CBs as follows Eq. 2.

$$DL(\%) = \frac{\text{Amount of total drug entrapped}}{\text{Total amount of } NCs} \times 100 \quad (2)$$

In-vitro drug release and release kinetic studies

The release performance of LTB and BCA from PLGA NPs and CBs was assessed by employing the dialysis bag method. The cellulose membrane having a molecular cut-off of 12 kDa was used for the study. Before the experiment, the membrane was activated using a 1% EDTA solution. After activation of the membrane, 2 mL of each NCs (PLGA and CBs) was taken in the dialysis membrane and closed from both ends utilizing dialysis closure clips. The dialysis bag was placed in physiological relevant media having pH 6.8, temperature 37 ± 0.5, and 100 rpm speed. An aliquot of 1 mL was withdrawn at different time intervals, and the same amount was replaced to maintain the sink conditions. The samples were analyzed for LTB and BCA using the RP-HPLC method. The amount of drug release from polymeric and lipidic NCs was calculated according to encapsulated drugs in both NCs. The data obtained were further evaluated by employing DD-solver software for drug release kinetics. In-vitro release kinetic studies were conducted assessing the regression coefficient values, Akaike information criterion (AIC) values, and release rate constant values (K) for zero-order, first-order, Higuchi, Hixson–Crowell model, and Korsmeyer–Peppas models [36, 38, 39].

Statistical analysis

The resulting data were expressed as mean ± standard deviation (SD). The data analysis was done through GraphPad Prism 9.1.0. (GraphPad software, United States America), Design Expert (13.0.5.0) and DD solver software. A statistically significant value was less than 0.05 in the whole experiment.

Results
Analytical method development and validation
Selection of wavelength
The $\lambda_{\max}$ for LTB and BCA was found at 248 nm and 260 nm when scanned individually in UV–Vis spectrophotometer (UV-2600, Shimadzu, Japan). The isosbestic point for both drugs was found at 253 nm (Additional file 1: Fig. S1), giving maximum absorbance. All the measurements in the RP-HPLC were made at 253 nm (isosbestic point).

RP-HPLC method development
The quadratic design models from the Box–Behnken design type (Version 13.0.5.0) were employed for all the resulting responses. The model was decided based on p-value, F-value, and adjusted R^2 values for each response (R1—area of LTB, R2—area of BCA, R3—peak resolution, R4—tailing factor of LTB, and R5—tailing factor of BCA). The p-values, F-value, and R^2 values for $R1$, $R2$, $R3$, $R4$, and $R5$ were found significant {(R1; 0.0115, 8.03, and 0.91), (R2; 0.0153, 7.18, and 0.9252), (R3; 0.0332, 5.22, and 0.9410), (R4; 0.0001, 52.26, and 0.9453), and (R5; 0.001, 63.44, and 0.951)}. The quadratic model was validated employing normal plots of residuals and residual vs predicted plots (Additional file 1: Fig. S2). The plots depicted no such significant deviation from the center line of the normal plot explaining the linearity. The residue is not only randomly distributed on each side of the zero line but also falls within the range of 2 (even lower than the permissible range of 3). Therefore, the finding of such distribution suggested linear model is appropriate, devoid of systematic error and suitable for use in optimizing the RP-HPLC method.

The analysis of variance was employed to study the significant terms (factors) using p-value and F-value. The ANOVA tables (Additional file 1: Tables S1–S5) for each response resulted from variation in significant factors $R1(A, B, AB, B^2)$, $R2(A, B, C, AB, A^2, B^2)$, $R3(A, B, AB, B^2,$ and $C^2)$, $R4(A, C, AC, B^2, C^2)$, and R5(A, C, AC, B^2, C^2) with p and F-values for each factor < 0.05 and > 5. To explain the unit correlation of each factor with their responses, the coded equations were obtained with high-level factors (+ 1) and low levels of factors (− 1).

$$\begin{aligned} R1 = &+ 1021 + 233.37A - 502.04B - 55.81C \\ &- 350.20AB + 12.75AC + 87.63 \\ &- 111.39A^2 + 325.84B^2 + C^2 \end{aligned} \quad (3)$$

$$\begin{aligned} R2 = &+ 1423 + 366.42A - 549.8B - 133.35C \\ &- 450AB - 4.05AC + 177.75BC \\ &- 227.04A^2 + 275.10B^2 - 74.85C^2 \end{aligned} \quad (4)$$

$$R3 = +\ 7.65 - 1.96A - 4.04B - 0.123C$$
$$+\ 1.84AB + 0.015AC - 0.107BC \qquad (5)$$
$$-\ 0.826A^2 + 0.98B^2 - 1.03C^2$$

$$R4 = +\ 1.16 - 0.0875A - 0.0112B + 0.243C$$
$$+\ 0.0175AB + 0.137AC + 0.070BC \qquad (6)$$
$$-\ 0.075A^2 + 0.102B^2 + 0.407$$

$$R5 = +\ 1.21 - 0.078A - 0.0513B + 0.225C$$
$$+\ 0.0300AB - 0.1375AC + 0.0325BC \qquad (7)$$
$$+\ 0.040A^2 - 0.105B^2 + 0.422C^2$$

The coded equation depicted a correlation among the responses (R1–R5) where positive sign (+) displayed factors are directly correlated to responses and negative sign (−) displays indirectly correlated values. The increase in mobile phase ratio increases the area of LTB and BCA as shown in the (Eq. 3) owing to more solubility of LTB and BCA in ACN than water. An indirect correlation between flow rate, pH of an aqueous phase, and area of both drugs was displayed (Eqs. 3, 4). The lower flow rate gives enough time for the analyte to interact with the stationary phase, thus producing more retention with more area and inverse in case of higher flow rate. It also affects the peak resolution based on their solubility differences with the mobile phase. As given in Eqs. 3–6 negative correlation was established among flow rate, pH, and area of LTB, BCA, and peak resolution. The pKa of LTB and BCA was 5.05 and 6.5; thus, according to the rule of pH ± 2 from pKa the pH of the aqueous phase was selected. At pH closer to the pKa of the drugs, both drugs

were in ionized fraction and thus reduction in pH up to 4 offered a higher area for both drugs. However, more reduction in < pH 4 makes BCA ionized, thus produced with a lesser area. The higher pH was found to produce peaks with more tailing factors than the lower pH. Thus, pH of the aqueous phase affects the area and tailing factors of LTB and BCA significantly (Eqs. 6, 7).

Visualization of data

The correlation of each factor with responses of RP-HPLC parameters was established. Though, the additive correlation was established by employing two factors at a time and response. The significant factors were taken in such response surface methodology (RSM) studies. Five different RSM plots were obtained explaining the additive correlation among factors and responses. As shown in Fig. 2A, B, a steep increase in the slope of the graph can be observed depicting a positive correlation with factors A and B. Figure 2C depicts a positive correlation among mobile phase, flow rate, and peak resolution. As already described, a decrease in pH and a higher mobile phase ratio of ACN reduces the tailing factor of both peaks as depicted in Fig. 2D, E.

Optimization

After variations in chromatographic conditions, several chromatograms were obtained with different retention times, resolution, separation factors, asymmetrical factors, and areas according to the solutions generated from BBD. The overlay plots from factors A, B, and C were obtained in Fig. 3A, B, exhibiting probable solutions according to our desirability. The chromatograms
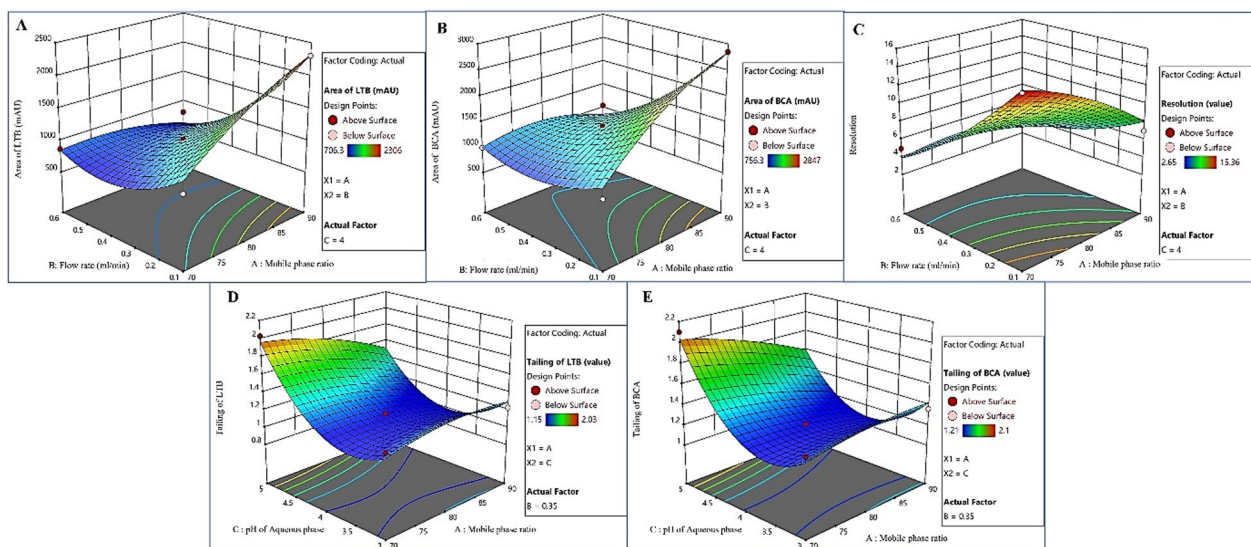
Fig. 2 3D-Response surface plots depicted the correlation between the significant factors and responses **A**. Area of LTB (R1) versus AB, **B**. Area of BCA (R2) versus AB, **C**. Peak resolution (R3) versus AB, **D**. Tailing of LTB (R4) versus AC, and **E**. Tailing of BCA (R5) versus AC
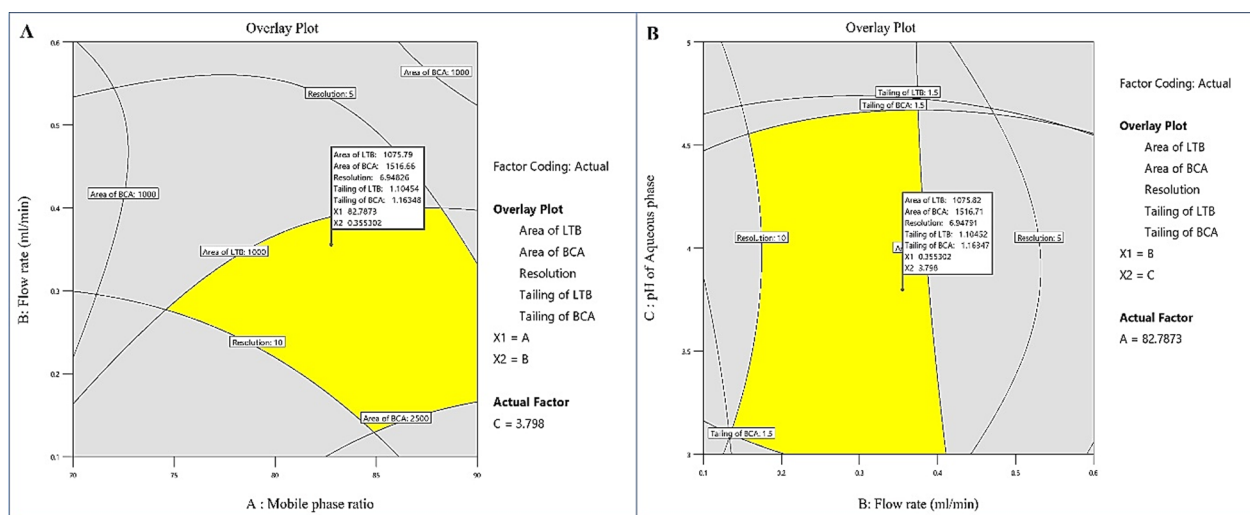
Fig. 3 Optimization of factors (A–C) for their desired responses **A**. Overlay plot of factor AB for their solutions **B**. Overlay plot of factor BC for their solutions

with the higher area, more resolution (>4), lesser asymmetrical factor (<1.5), and more theoretical plates number (>5000) were considered for method development among all solutions [29]. The desirability of each response can be achieved using a mobile phase ratio between 83:17 and 86:15, flow rate 0.35–0.4 mL/min, and pH of aqueous phase 3.5–4.

The finally optimized chromatograms for BCA and LTB (Fig. 4A) were obtained at conditions suggested using BBD as mobile phase ratio (Acetonitrile: Acidified water pH 4) 85: 15, flow rate 0.4 mL/min at 30 °C column temperature conditions. The responses were recorded as (R1) area of LTB 1071 ± 53.66 and (R2) area of BCA 1422 ± 16.28, (R3) peak resolution 6.61 ± 0.007, (R4) Tailing factor of LTB chromatogram 1.153 ± 0.011 and (R5) Tailing factor of BCA chromatogram 1.116 ± 0.02. The 10 µl volume of both drugs in different concentrations was injected that retained on the stationary phase (YMC-Pack Pro C18, 150 × 4.6 mm L.D. S-5 µm,12 nm) at R_t 4.09 min (BCA) and 5.15 min (LTB) to give a straight line for quantification of known concentrations.

Assay validation
Linearity and range
The standard calibration curve was plotted for both drugs and found to be linear over the concentration range of 0.5–32 µg/mL. The coefficient of linear regression (R^2) for LTB was found to be 0.9998 with its linear equation y = 153.43x-15.202 (Fig. 4B). However, linear regression analysis of BCA resulted in an R^2 value of 0.997 with its linear line equation y = 93.987x + 11.254 (Fig. 4B).

Accuracy
Accuracy is the degree of closeness between observed values and standard values and is generally expressed as percentage recovery. The quality control samples (LQC, MQC, and HQC) for LTB and BCA exhibited higher % recovery in the range of (94–103%) as given in Table 3. The % average bias (difference from standard value) results depicted acceptable values, i.e., ± 5%, thus confirming the accuracy of the proposed method for the quantification of both drugs simultaneously.

Precision
The precision can be assessed utilizing % RSD values that determine the existence of random error on repeatability. The data from quality control samples (LQC, MQC, and HQC) of both drugs were analyzed for % RSD, % accuracy, and % average bias for their intra-day and inter-day precision determination. Table 4 explains the intra-day precision values that were found to be in the acceptable range of < 2% RSD and ± 5% average bias.

The values from inter-day (3 consecutive days) precision calculations in Table 5 depicted lower values of % RSD (<2) and % average bias (± 5). The overall findings from precision determination (intra-day and inter-day) demonstrated the proposed RP-HPLC method is more precise for determining LTB and BCA simultaneously [29, 31, 32].

Sensitivity
The standard error (SE) intercept for LTB and BCA from their calibration curve was found to be 0.164 and 0.085, respectively. The values were further calculated to give
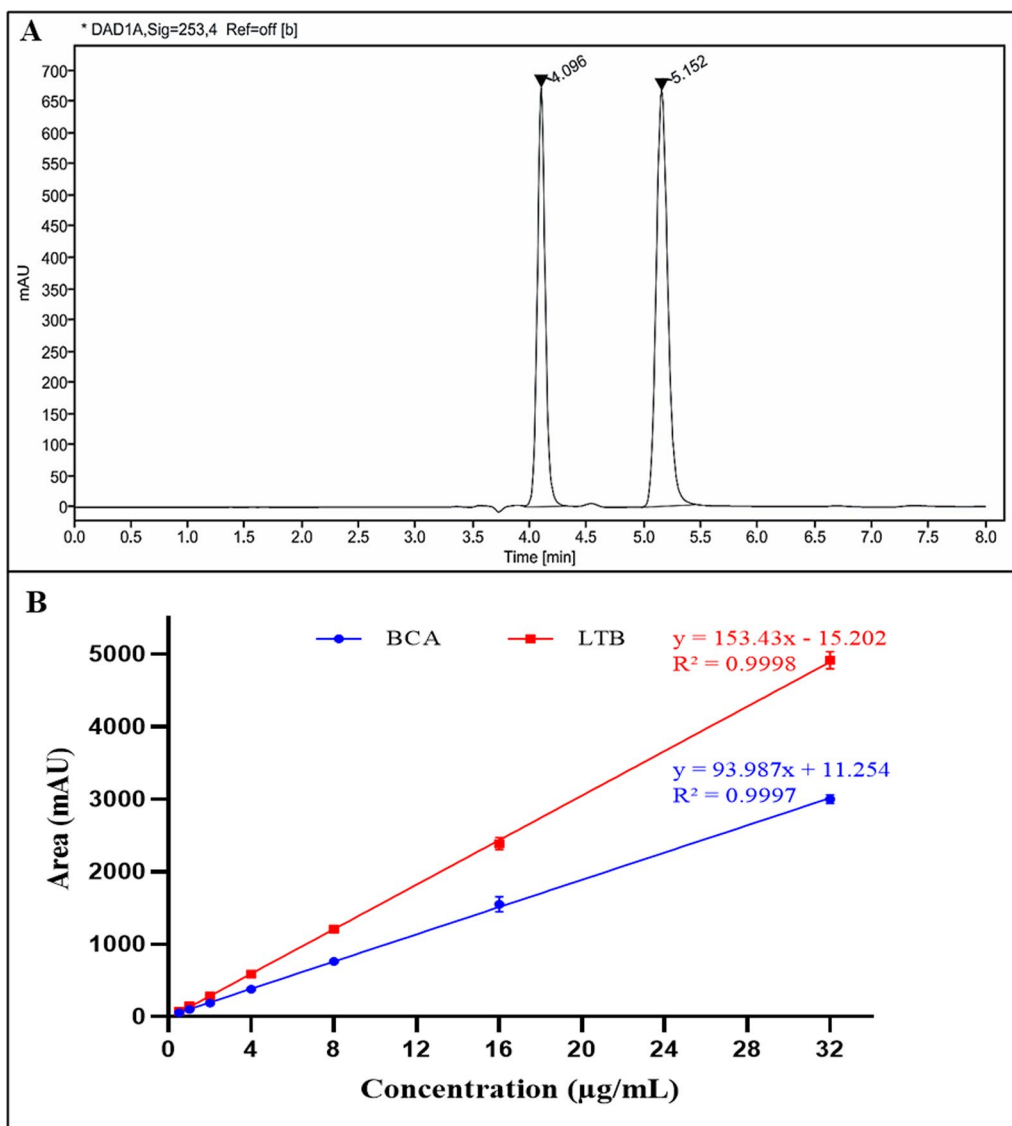
Fig. 4 **A**. Chromatograms of BCA and LTB at retention time 4.09 min and 5.15 min, respectively **B**. Standard calibration curves of BCA and LTB

Table 3 Accuracy values at different levels of the validated analytical method

Analytes	Actual concentration (µg/mL)	Observed concentration (µg/mL)	% Accuracy*	% RSD	Avg. % Bias
BCA	0.5	0.470	95.77 (± 1.28)	1.340	4.220
	4	3.980	99.50 (± 0.64)	0.640	0.490
	32	33.250	103.92 (± 1.90)	1.820	− 3.920
LTB	0.5	0.505	101.09 (± 1.86)	1.841	− 1.094
	4	3.781	94.53 (± 0.80)	0.842	5.473
	32	30.711	95.97 (± 0.67)	0.693	4.027

*Data expressed as mean ± SD, $n = 3$

Table 4 Intra-day precision values at different levels of the validated analytical method

Analytes	Actual concentration (µg/mL)	Observed Concentration* (µg/mL)	Intra-day precision %RSD	% Accuracy*	Avg. % Bias
BCA	0.5	0.495 (±0.006)	1.130	98.998 (±1.12)	1.002
	4	3.98 (±0.044)	1.102	99.499 (±1.1)	0.5015
	32	31.812 (±0.619)	1.947	99.413 (±1.94)	0.5874
LTB	0.5	0.518 (±0.007)	1.403	103.86 (±1.455)	−3.7763
	4	3.954 (±0.07)	1.927	98.86 (±1.905)	1.1392
	32	31.84 (±0.573)	1.800	99.51 (±1.791)	0.4894

*Data expressed as mean ± SD, $n = 3$

Table 5 Inter-day precision values at different levels of the validated analytical method

Analytes	Actual concentration (µg/mL)	Observed concentration*	Inter-day precision %RSD	% Accuracy*	Average bias
BCA (Day 1)	0.5	0.484 (±0.006)	1.154	96.862 (±1.11)	3.13
	4	3.916 (±0.044)	1.120	97.89 (±1.09)	2.10
	32	31.22 (±0.207)	0.662	97.563 (±0.64)	2.43
LTB (Day 1)	0.5	0.512 (±0.007)	1.421	102.46 (±1.45)	−2.46
	4	3.915 (±0.076)	1.946	97.87 (±1.90)	2.12
	32	31.209 (±0.573)	1.837	97.52 (±1.79)	2.47
BCA (Day 2)	0.5	0.4740 (±0.005)	1.180	94.501 (±1.11)	5.18
	4	3.95 (±0.043)	1.109	98.87 (±1.097)	1.12
	32	30.80 (±0.1514)	0.491	96.271 (±0.47)	3.72
LTB (Day 2)	0.5	0.506 (±0.007)	1.438	101.21 (±1.45)	−1.21
	4	3.939 (±0.076)	1.934	98.479 (±1.90)	1.52
	32	31.04 (±0.573)	1.847	97.004 (±1.79)	2.99
BCA (Day 3)	0.5	0.494 (±0.005)	1.131	98.86 (±1.11)	1.13
	4	3.958 (±0.043)	1.108	98.96 (±1.09)	1.03
	32	32.15 (±0.209)	0.650	100.48 (±0.63)	−0.48
LTB (Day 3)	0.5	0.518 (±0.072)	1.404	103.69 (±1.45)	−3.69
	4	3.9414 (±0.076)	1.933	98.536 (±1.90)	1.46
	32	30.816 (±0.282)	0.918	96.30 (±0.88)	3.69

*Data expressed as mean ± SD, $n = 3$

LOD and LOQ for LTB at 0.01 µg/mL and 0.030 µg/mL, while the LOQ and LOD for BCA were determined to be 0.008 µg/mL and 0.025 µg/mL, respectively. The measured values are sufficient for detecting and quantifying LTB and BCA with accuracy and precision.

$$\text{LOD} = 3.3 \times (\text{Standard deviation of intercept/Slope})$$
$$\text{LOQ} = 10 \times (\text{Standard deviation/Slope})$$

Robustness
The results shown in Table 6 confirmed the robustness of the proposed RP-HPLC method with no significant difference in resolution, tailing factor, and theoretical plate number values. The finding from the study reflects the reliability of the robustly developed method for estimating two drugs concurrently.

System suitability
After 10 µg/mL injection of both drugs, the well-resolved chromatograms with their R_t values at 4.09 min for BCA and 5.15 min for LTB were obtained, having a resolution value of 6.61 ± 0.007. The tailing factor played an important role in explaining the symmetry of the peak and was found to be within acceptable limits of < 1.5, according to USP. All the other parameters of RP-HPLC, i.e., theoretical plates and height equivalent to theoretical plates (HETP), were found to be acceptable limits as shown in Table 7. The results from such

Table 6 Robustness of the validated analytical method

Analyte	Concentration (µg/mL)	Resolution*	Tailing*	Theoretical plates*
Optimized parameters: 4.0 pH, 0.4 mL/min flow rate, 85:15 mobile phase ratio, and column temperature 30 ℃				
BCA	0.5	–	1.10 (±0.026)	14,162 (±89.8)
	4	–	1.13 (±0.03)	14,642.6 (±24.3)
	32	–	1.065 (±0.005)	17,226 (±23.6)
LTB	0.5	6.53 (±0.021)	1.16 (±0.01)	11,863 (±7.54)
	4	6.60 (±0.005)	1.16 (±0.005)	12,042 (±38.09)
	32	6.70 (±0.006)	1.17 (±0.021)	12,424 (±22.91)
Change in pH 3.5				
BCA	0.5	–	1.16 (±0.038)	15,173 (±97)
	4	–	1.12 (±0.01)	15,095 (±100)
	32	–	1.124 (±0.016)	17,199.3 (±10.61)
LTB	0.5	5.91 (±0.17)	1.07 (±0.03)	12,822.6 (±33)
	4	6.34 (±0.17)	1.15 (±0.017)	12,757.3 (±130.7)
	32	6.76 (±0.03)	1.15 (±0.015)	12,819 (±12.5)
Change in pH 4.5				
BCA	0.5	–	1.087(±0.08)	13,819 (±111)
	4	–	1.153 (±0.03)	14,049 (±68)
	32	–	1.117 (±0.021)	16,522 (±139)
LTB	0.5	6.53 (±0.05)	1.34 (±0.03)	12,297 (±78.42)
	4	6.6 (±0.02)	1.16 (±0.03)	12,331.3 (±57.3)
	32	6.76 (±0.034)	1.17 (±0.03)	12,612 (±99.14)
Change in flow rate of mobile phase: 0.38 mL/min				
BCA	0.5	–	1.104 (±0.043)	1444 (±13.11)
	4	–	1.141 (±0.017)	14,757 (±30.805)
	32	–	1.078 (±0.051)	17,210.93 (±6.957)
LTB	0.5	6.687 (±0.001)	1.153 (±0.038)	12,098.3 (±18.823)
	4	6.673 (±0.005)	1.1736 (±0.040)	12,294.6 (±32.02)
	32	6.864 (±0.018)	1.1673 (±0.011)	12,653 (±60.32)
Change in flow rate of mobile phase: 0.42 mL/min				
BCA	0.5	–	1.128 (±0.007)	14,030 (±18.248)
	4	–	1.224 (±0.035)	14,030 (±18.24)
	32	–	1.109 (±0.046)	16,689 (±103.79)
LTB	0.5	6.522 (±0.008)	1.140 (±0.027)	12,239.67 (±37.44)
	4	6.592 (±0.038)	1.1894 (±0.060)	12,253.3 (±74.14)
	32	6.787 (±0.025)	1.1738 (±0.0182)	12,572 (±62.628)
Change in mobile phase ratio: 83: 17% (ACN: Acidified water)				
BCA	0.5	–	0.910 (±0.009)	16,352 (±19.38)
	4	–	1.115 (±0.022)	14,738.6 (±36.82)
	32	–	1.124 (±0.016)	17,199.3 (±10.61)
LTB	0.5	7.727 (±0.071)	1.108 (±0.048)	12,332.6 (±12.61)
	4	7.537 (±0.020)	1.139 (±0.018)	12,210.6 (±43.775)
	32	7.777 (±0.023)	1.1392 (±0.027)	12,496.3 (±28.676)
Change in mobile phase ratio: 87: 13% (ACN: Acidified water)				
BCA	0.5	–	1.029 (±0.067)	15,617 (±17.16)
	4	–	1.115 (±0.0264)	15,453.66 (±19.25)
	32	–	1.092 (±0.020)	16,853.6 (±14.08)
LTB	0.5	5.957 (±0.037)	1.139 (±0.019)	12,790.3 (±15.42)
	4	5.902 (±0.014)	1.1623(±0.0297)	12,712.66 (±57.23)
	32	5.999 (±0.02)	1.160 (±0.0297)	12,917 (±11.53)

Table 6 (continued)

Analyte	Concentration (µg/mL)	Resolution*	Tailing*	Theoretical plates*
Change in column temperature 28 °C				
BCA	0.5	–	0.90 (±0.02)	16,361 (±79.03)
	4	–	1.11 (±0.01)	15,178.8 (±59.3)
	32	–	±0.01)	17,245 (±86.5)
LTB	0.5	6.90 (±0.05)	1.15 (±0.04)	12,101 (±26.3)
	4	6.86 (±0.01)	1.15 (±0.03)	12,479.6 (±73.07)
	32	7.023 (±0.0321)	1.157 (±0.024)	12,748 (±7.63)
Change in column temperature 32 °C				
BCA	0.5	–	0.92 (±0.01)	16,405 (±76.3)
	4	–	1.109 (±0.026)	15,100.8 (±57.9)
	32	–	1.08 (±0.032)	16,927 (±55.03)
LTB	0.5	6.77 (±0.082)	1.14 (±0.02)	12,396.7 (±41)
	4	6.59 (±0.01)	1.149 (±0.013)	12,268.9 (±46.5)
	32	6.701 (±0.002)	1.14(±0.015)	12,545 (±96.26)

*Data expressed as mean±SD, *n*=3

Table 7 System suitability parameter of the validated analytical method

Analyte	Retention time *(Min)	Peak resolution* (*R*)	Theoretical plates* (*N*)	Tailing*	Separation factor	HETP* (mm)
BCA	4.085 (±0.0005)	–	14,895.06 (±50.84)	1.116 (±0.02)	–	0.01 (±0.0001)
LTB	5.14 (±0.003)	6.61 (±0.007)	12,168.24 (±16.37)	1.153 (±0.011)	1.259 (±0.001)	0.012 (±0.0001)

*Data expressed as mean±SD, *n*=6

observation depicted the system suitability of the validated analytical method.

Application of RP-HPLC method in drug degradation studies

Quantification of force-degradant products using RP-HPLC and HRMS

The degradation behavior for both drugs under acidic, basic hydrolytic, and oxidative conditions was reported through % recovery, as shown in Table 8. The individual drugs were accessed for each degradant by use of RP-HPLC. In the case of LTB, major degradation was found in basic hydrolytic and oxidative conditions with

Table 8 Percentage recovery of LTB and BCA after different stress conditions

Stress conditions	Sample treatment	LTB % recovery*	BCA % recovery*
Acidic hydrolysis	0.1N HCL	97.39 (±8.43)	94.7 (±6.28)
Basic hydrolysis	0.1N HCL	57.79 (±7.9)	78 (±3.17)
Neutral hydrolysis	H_2O	102.5 (±1.78)	85.52 (±6.68)
Oxidation	H_2O_2	59.25(±3.9)	92.7 (±5.26)

*Data expressed as mean±SD, *n*=3

percentage recovery of 57.79±7.9 and 59.25±3.9%. The degradants found in LTB were observed to be retained on the stationary phase of RP-HPLC (Fig. 5A1–D1) explains the specificity of the proposed method for LTB.

However, BCA undergoes basic and oxidative degradation to a more considerable extent. The results from the oxidative degradation study showed that BCA undergoes an oxidative coupling reaction. The observed degradants of BCA were found to be quantified through the developed RP-HPLC method with a peak resolution of more than 1.5 (Fig. 5A2–D2), thus supporting the specificity of the method.

HRMS studies of LTB, BCA, and their DPs

The study employed to find the major degradants of LTB and BCA after stress conditions. LTB and BCA showed protonated ions at *m/z* 427.11 and 285.07, respectively, depicting the characteristic *m/z* according to the literature. Further, HRMS analysis of respective LTB and BCA was performed. The LTB shows (Fig. 6A) a base peak at *m/z* 427.11, with its major fragments (*m/z* 410.34, 392.06, 370.05, 355.0, 338,327, and 312.02) [40]. The prediction model (Zeneth) depicted the total
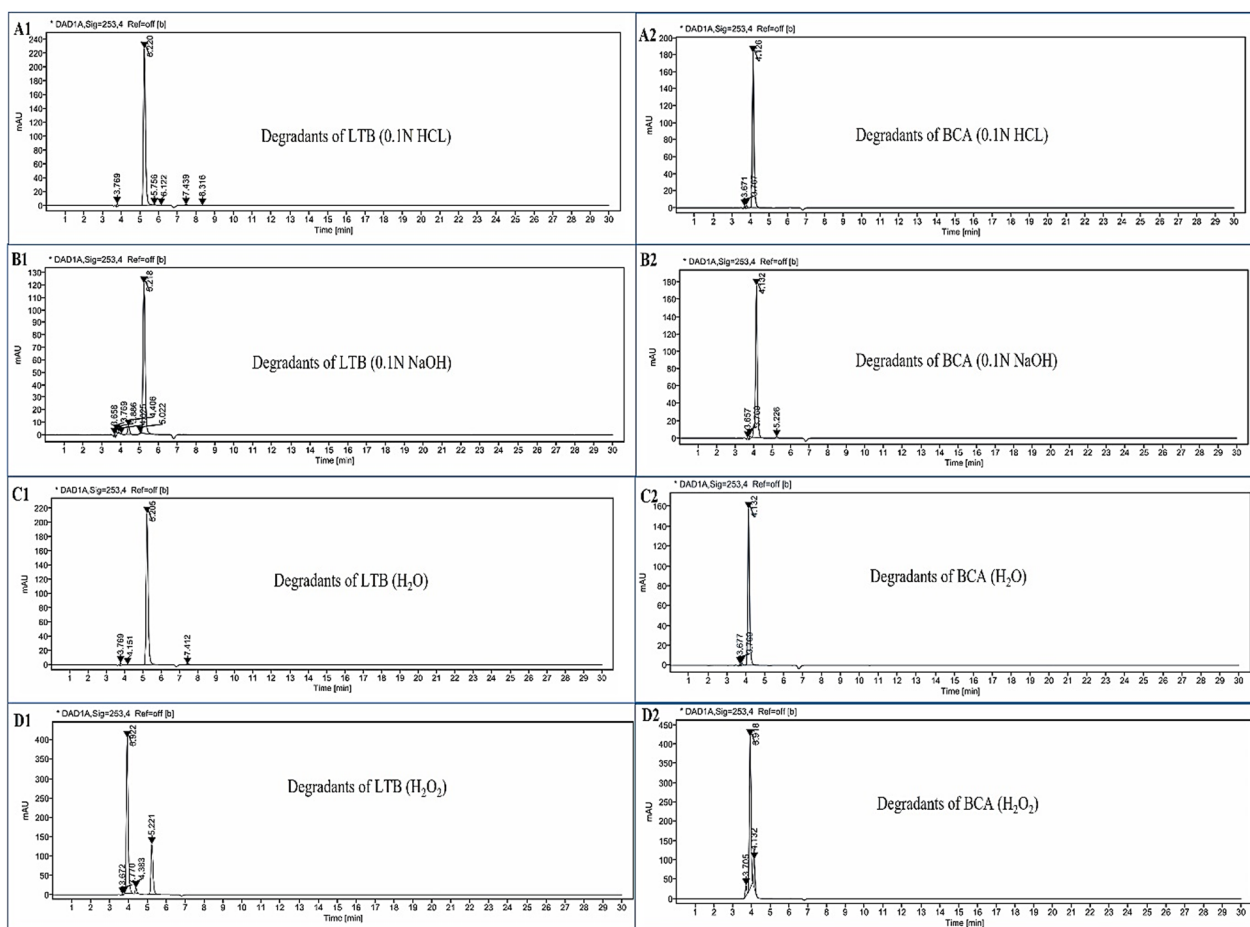
Fig. 5 Chromatograms obtained after **A1-2**. Acidic (0.1N HCL) **B1-2**. Basic (0.1N NaOH), **C1-2**. Neutral (H_2O) and **D1-2**. Oxidative (3% H_2O_2) treatment of LTB and BCA at 80 °C for 2 h

eighteen degradants of LTB, namely LD1–LD18, under different stress conditions, as shown in Table 1. However, experimentally, seven major degradants were quantified through their *m/z* charge ratio i.e., related to the degradant average mass (Fig. 6A–H). The mass accuracy error was found to be < 10 ppm for each degradant.

The observed degradants were LD1, LD4, LD5, LD6, LD11, LD14, and LD16 having *m/z* ratios 58.06, 102.05, 445.12, 227.05, 144.02, 418.04, and 595.08 respectively. Briefly, all the degradants were formed due to the loss or gain of molecular mass from parent ions (LTB) or daughter ions (degradants) (Additional file 1: Fig. S3). The FDS caused parent ions to generate four major degradants with their loss in the molecular formula from LTB as LD1 formed due to loss of—$C_{18}H_{12}ClN_3O_4$ from LTB, similarly LD4;—C_4H_5NO, LD5;—HN, and LD6;—$C_{11}H_8N_2O_2$ {here, (−) sign indicates loss of molecular formula and (+) sign indicates gain of molecular formula}. The formation

of LD11, LD14 and LD16 were driven by the loss of– $C_4H_6N_2$ from LD3,–$C_{10}H_{10}ClN_3$ from LD5, and addition+C_7H_3NO from LD6. More studies using NMR analysis need to be conducted in the future to further characterize each degradant [34, 41].

A total of twenty-four BCA degradants (BD) were obtained with their mass error value < 10 ppm. The BCA degrades owing to hydrolysis or coupling reactions between the degradants. Different isoforms consisting of similar molecular average mass or formulas and different structures were examined. The average mass of degradants was found for each degradants as BD4: 566.51, BD5: 566.51, BD6: 566.51, BD14: 848.76, BD15: 848.76, BD16: 1131.1, BD17: 1131.1, BD18: 848.76, BD19: 1131.1, D20: 564.5, BD21: 564.5, BD22: 580.5, BD23: 580.5, BD24: 580.5, BD25: 580.5, BD26: 580.5, BD27: 848.76, BD28: 1131.01, BD29: 564.5, BD30: 580.5, BD31: 1131.01, BD32: 564.5, BD33: 564.5, and BD34: 564.5 (Fig. 7B–F).
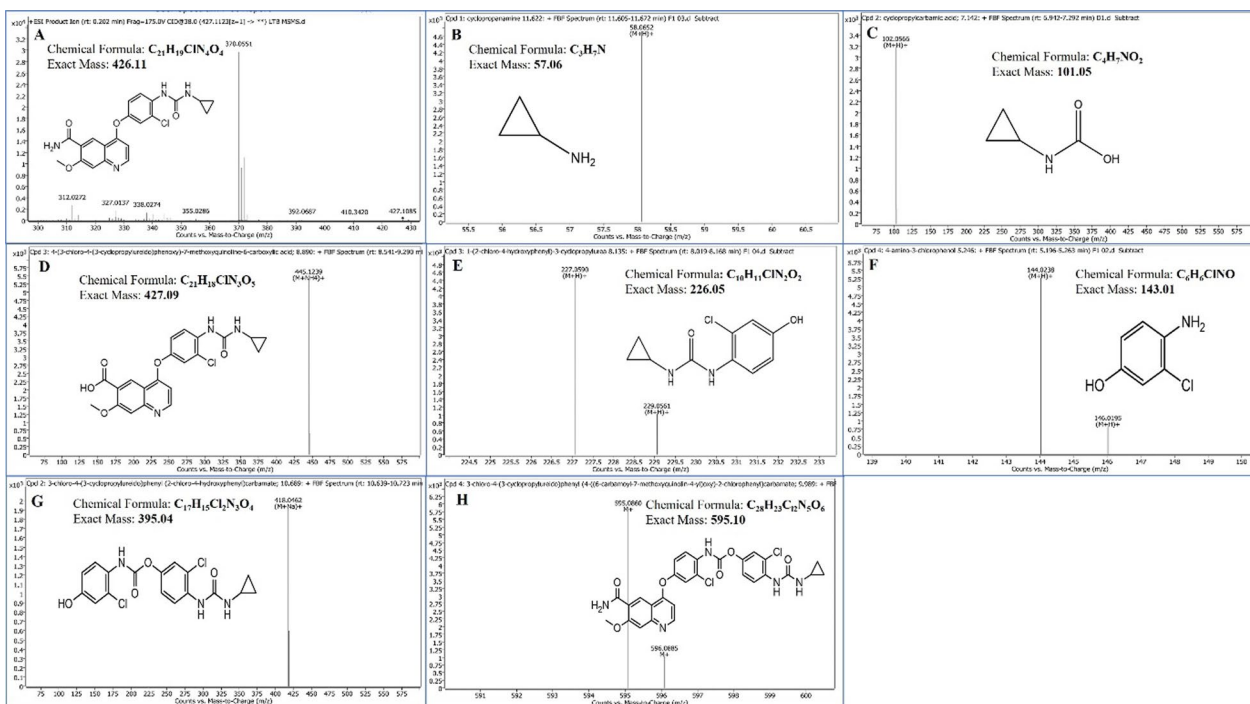
Fig. 6 HRMS spectra of (**A**) LTB (**B**) LD1, (**C**) LD4, (**D**) LD5, (**E**) LD6**,** (**F**) LD11, (**G**) LD14 and (**H**) LD16
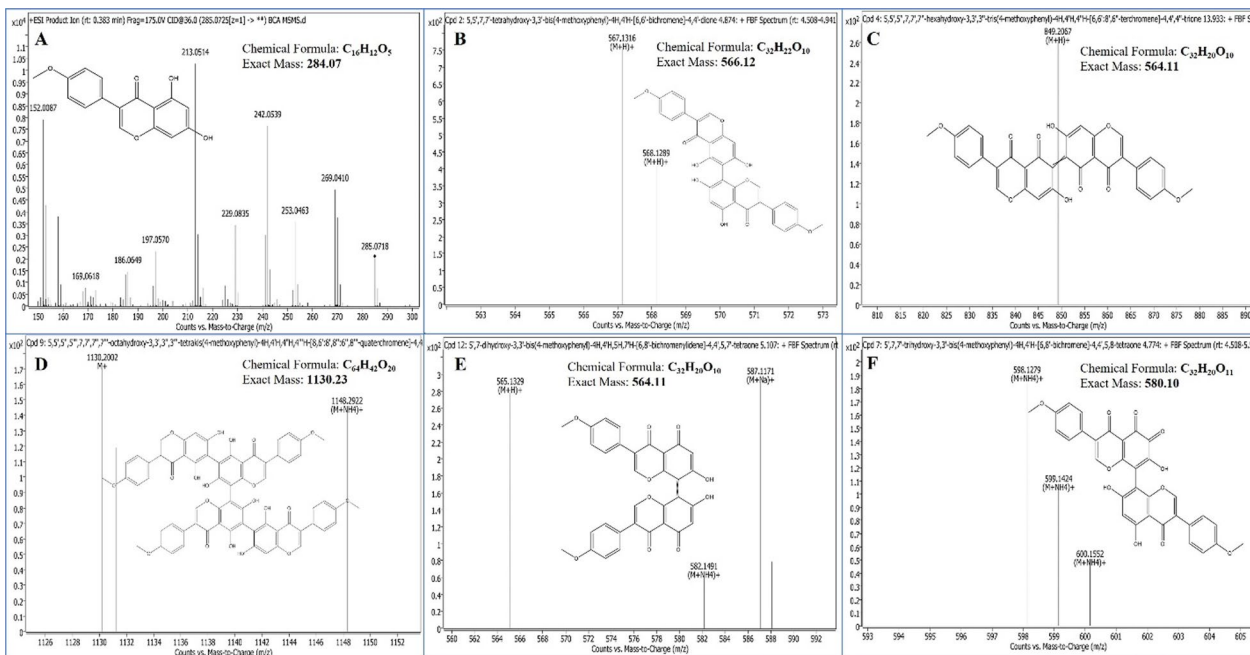
Fig. 7 HRMS spectra of (**A**) BCA (**B**) BD4, BD5, and BD6 (**C**) BD14, BD15, BD18, and BD27 (**D**) BD16, BD17, BD19, BD28, BD31 (**E**) BD20, BD21, BD29, BD32, BD33, and BD34 (**F**) BD22, BD23, BD24, BD26, and BD30

The types of degradants were formed due to coupling reactions among the degradants, as also illustrated in the in silico prediction study. A better understanding of each degradant for its isomers can result from an NMR study in the future.

In this study, to explain the underlying mechanism of each degradant, major common degradants with their average masses were considered from their parent moieties as depicted in (Additional file 1: Fig. S4).

The degradants D4, D5, and D6 with molecular mass at *m/z* ratio 566.51 were formed due to the addition of $+C_{16}H_{10}O_5$ in the parent BCA moiety. The degradants with an average mass of 848.76 *m/z*, i.e., BD14, BD15, BD18, and BD27, were formed owing to oxidation coupling of phenol $(C_{32}H_{20}O_{10})$ with parent BCA and degradants (D4, and D5). The degradants (BD16, BD17, BD19, BD28, BD31) with an average mass of 1131.01 were formed owing to the oxidation coupling between $C_{48}H_{30}O_{15}$ and degradants D4, D5, and D6 individually. An average mass of 564.5 at their *m/z* resulted in degradants (BD20, BD21, BD29, BD32, BD33, and BD34) due to the oxidation of biphenyldiol to biphenyldione with a gain of molecular formula $(C_{16}H_8O_5)$ in D4, D5, and D6. Finally, degradants (BD22, BD23, BD24, BD26, and BD30) with an average mass of 580.5 at *m/z* were formed owing to oxidation coupling between $C_{16}H_8O_6$ and degradants D4, D5, and D6 individually[33, 34, 41].

In-silico degradation toxicity

The in-silico and experimental observations reported different degradants for the LTB and BCA. The Derek analysis using different animals models resulted in numerous toxicities for drugs and their derivatives. A total of eighteen drug alerts were found from in silico toxicity studies for BCA. However, LTB possesses only two drug alerts for their derivatives (Additional file 1: Table S6).

Development of drug nanocarriers
Selection of solvent

The saturation solubility of BCA and LTB was determined to select the best possible solvent to formulate the PLGA NPs. The solubility of BCA in water, methanol, acetone, acetonitrile, DMF, ethanol, DCM, and DMSO were found to be 0.007 ± 0.003 mg/mL, 9.90 ± 0.15 mg/mL, 26.48 ± 0.15 mg/mL, 13.27 ± 0.19 mg/mL, 24.83 ± 0.32 mg/mL, 12.03 ± 1.047 mg/mL, 1.34 ± 0.003 mg/mL, and 33.87 ± 1.74 mg/mL respectively (Fig. 8). However, the solubility of LTB in the same solvents was determined as 0.57 ± 0.146 mg/mL, 4.93 ± 0.44 mg/mL, 1.19 ± 0.049 mg/mL, 0.17 ± 0.244 mg/mL, 3.33 ± 0.33 mg/mL, 0.72 ± 0.075 mg/mL, 0.63 ± 0.08 mg/mL, and 10.56 ± 0.209 mg/mL respectively (Fig. 8).

The cosolvents acetone and methanol were used to prepare the PLGA NPs owing to the higher solubilities of drugs and polymers. However, methanol was adopted as a solvent to dissolve the lipid, LTB, and BCA during the production of CBs.

Particle size, PDI, and zeta potential

The particle size and zeta potential for PLGA NPs were found to be 185.3 ± 12.3 nm and -13.3 ± 0.35 mV Fig. 9A1, B1.

The particles were found to be of uniform size with a PDI value of 0.183 ± 0.06. However, CBs were observed to exhibit the 182.4 ± 16.3 nm aerodynamic particle size with a slight deviation in uniformity with a PDI value of 0.213 ± 0.05. The CBs were examined to possess -10.8 ± 0.39 mV zeta potential. The results from such findings depicted that the PLGA NPs and CBs were of uniform nanosized range particles.

% EE and %DL of LTB and BCA in PLGA NPs and cubosomes

The PLGA is well known to encapsulate the hydrophobic and hydrophilic drugs inside the matrix. The % EE of the LTB and BCA in PLGA NPs were found to be
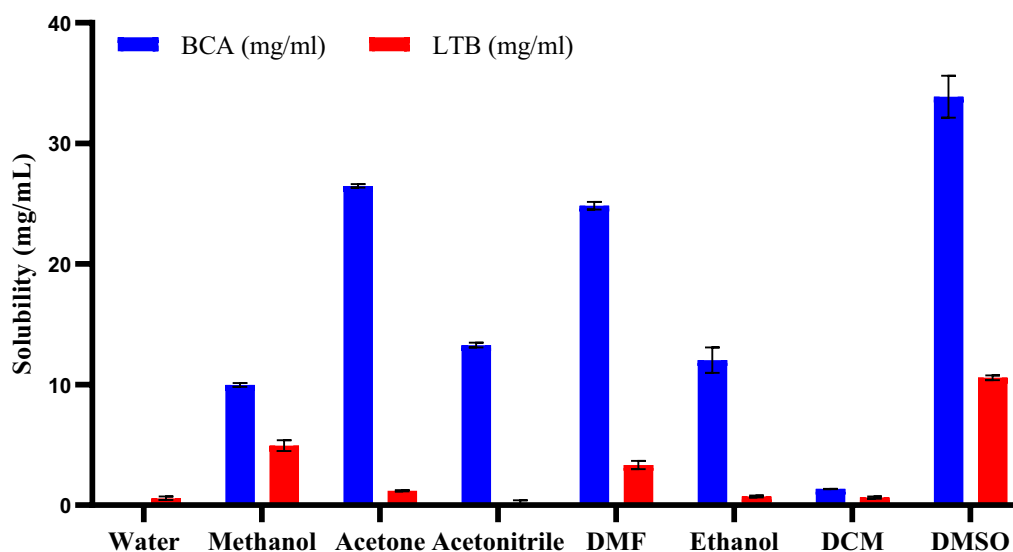

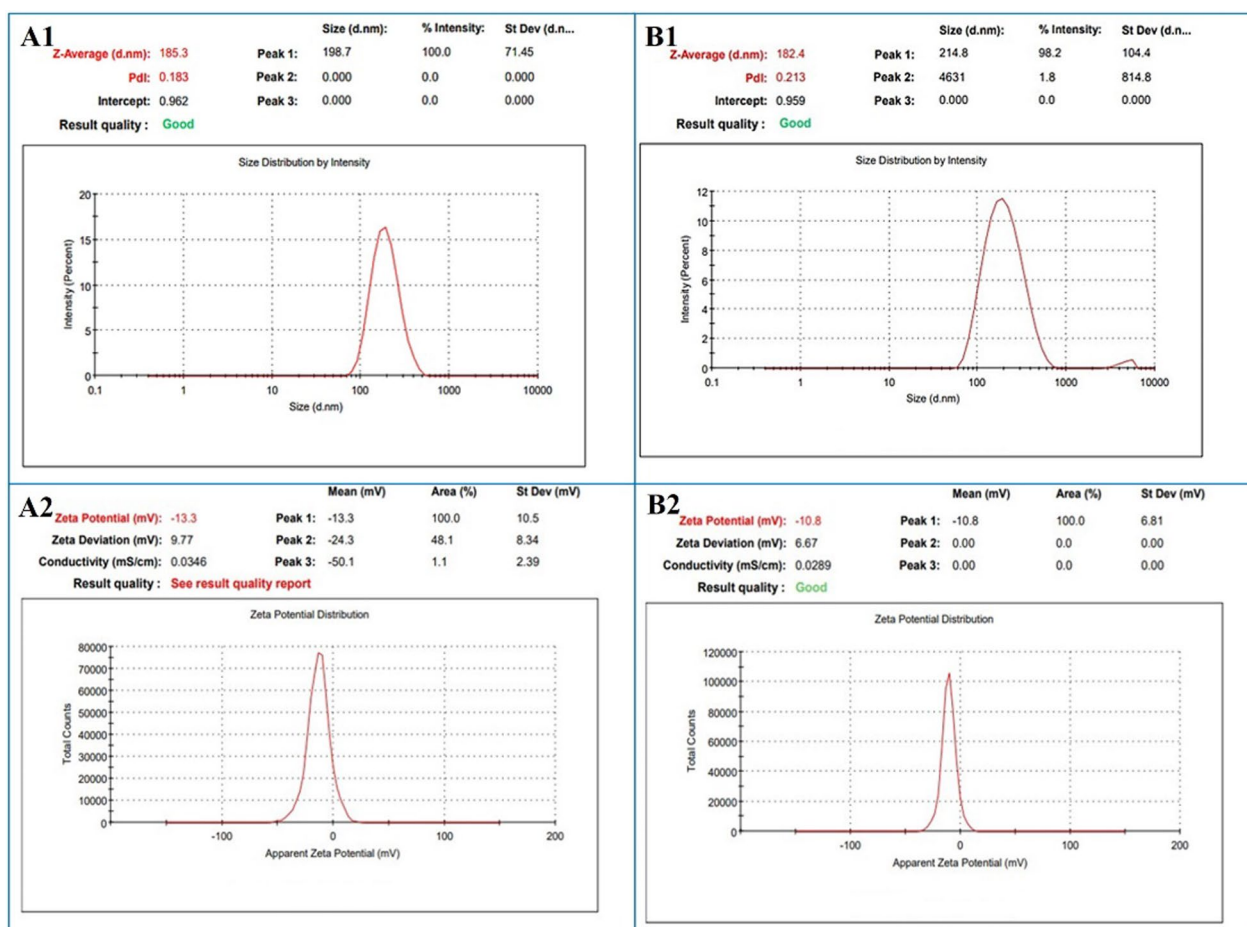**Fig. 8** Solubility determination of BCA and LTB in different solvents

Fig. 9 Particle size and zeta potential of **A1-2** PLGA NPs and **B1-2** CBs

$53.64 \pm 4.81\%$ and $61.29 \pm 4.67\%$, respectively. The higher % EE of BCA was examined owing to the inherent hydrophobic nature of the former. Additionally, it was discovered that both types of drugs were more effectively captured by the CBs, for that %EE of BCA was found to be $72.88 \pm 5.52\%$ and LTB was $55.62 \pm 7.73\%$. The housing that BCA and LTB were able to hold inside the carrier was provided by the liquid crystalline structure. The % DL was found to be $5.42 \pm 1.10\%$ and $4.43 \pm 0.77\%$ for BCA and LTB-embedded CBs, whereas PLGA NPs exhibited lower % DL with $3.7 \pm 0.46\%$ and $4.63 \pm 0.48\%$ content of BCA and LTB, respectively.

In-vitro drug release and kinetics studies

The quantification of LTB and BCA release from coarse suspension, polymeric, and lipidic nanocarriers at different time intervals was studied using RP-HPLC. The coarse LTB and BCA were found to show significant differences in release performance owing to the hydrophilic or hydrophobic nature of both drugs, as shown in Fig. 10A, B.

A long-sustained drug release effect for up to 72 h was observed from PLGA and CBs. However, a slight difference was observed in release performance and release kinetics of the LTB and BCA from PLGA NPs and CBs (Fig. 10A, B). BCA was found to exhibit a longer release pattern ($92.80 \pm 9.34\%$) due to the entrapment of hydrophobic content in the hydrophobic polymer (PLGA). It follows the first-order release kinetics mechanism from PLGA NPs with its highest regression coefficient (R^2) of 0.991 and AIC value of 40.46 with a 0.038 release rate constant (K). A faster LTB release ($73 \pm 4.9\%$ in 12 h) was observed from PLGA than BCA ($36 \pm 4.0\%$ in 12 h) owing to more hydrophilicity of the LTB than BCA. An LTB was found to obey the First-order release kinetics mechanism with R^2 0.934, AIC 59.23, and $K = 0.82$.

The CBs are well known to entrap hydrophilic and hydrophobic moieties in their core compartment region. LTB and BCA exhibited sustained release patterns from CBs with $95.30 \pm 6.6\%$ and $90.308 \pm 2.09\%$ release of BCA and LTB after 72 h, respectively. The release kinetics of BCA follows 1st order release mechanism with R^2 ;0.98,
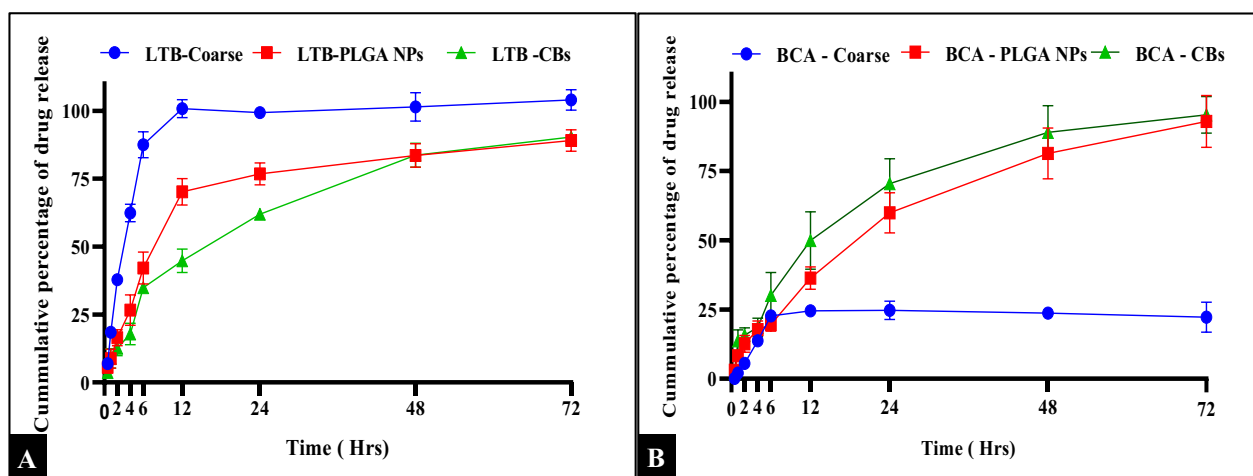
Fig. 10 In-vitro drug release **A**. Cumulative percentage of LTB release from Coarse-suspension of LTB, LTB- PLGA NPs, and LTB-CBs, **B**. Cumulative percentage of BCA release from Coarse-suspension of BCA, BCA- PLGA NPs, and BCA-CBs

Table 9 Release rate kinetics of BCA and LTB release from PLGA NPs and CBs

Models	BCA-PLGA			LTB-PLGA			BCA-CBs			LTB-CBs		
	R^2	AIC	K	R^2	AIC	K	R^2	AIC	K	R^2	AIC	K
Zero-order	0.81	68.43	1.535	0.23	81.32	1.602	0.65	75.06	1.66	0.67	73.36	1.56
1st order	0.991	40.46	0.038	0.934	59.23	0.82	0.985	46.28	0.055	0.97	51.58	0.46
Higuchi	0.98	48.44	11.10	0.82	68.20	12.47	0.96	54.44	12.33	0.972	51.19	11.53
Hixson–Crowell	0.972	49.37	0.010	0.865	65.64	0.019	0.969	53.33	0.015	0.940	58.04	0.013
Korsmeyer–Peppas	0.986	47.10	8.89	0.87	66.67	19.61	0.966	56.08	13.44	0.973	52.9	12.36

AIC ;46.28, and *K* ;0.055 values. However, LTB was found to follow the Higuchi model with the highest R^2 ;0.973, AIC ;51.19, and 11.53 release constant values (Table 9).

Discussion

The chemo-herbal combination approaches are the new era of cancer therapies. The use of protein-targeted drugs, namely tyrosine kinase inhibitors, in cancer treatments has been studied more. There are numerous FDA-approved TKI drugs for different types of cancers. However, side effects, organ toxicities at higher doses, and lower bioavailability restricted the anti-cancer potential of such bioactives. Herbal medicines has strengthened the therapeutic profiles of various chemotherapeutics [1]. BCA has shown prominent results as a combination therapy among various herbals due to its anti-cancer and anti-inflammatory activities. Youssef et al., in their study, introduce the novel chemo-herbal combination using BCA and sorafenib (multiple tyrosine kinase inhibitors) for effective anti-proliferative and apoptotic effects. Findings from the studies elaborated

the role of BCA in combination with other chemotherapeutics to potentiate the anti-cancer effect, reduce normal cell toxicities, make cost-effective treatments, and make future scopes for combination therapies [14].

The QbD systemic approach explains how method variables can affect the critical analytical attributes (CAAs). To aim the quality target method profile (QTMP), the considered CAA, i.e., the area of LTB and BCA, represents the concentrations of each drug, resolution time reflects the degree of separation of two adjacent peaks, and the tailing factor explains the efficiency of the method [42].

The p-value, F-values from the ANOVA table (Additional file 1: Tables S1–S5), coded equations, and 3D visualization of data by surface responses establish a correlation among each factor and responses. The overlay plots of designs depicted probable solutions according to our desirability of the results. The developed RP-HPLC method was validated for linearity, accuracy, precision, sensitivity, robustness, and system suitability.

The therapeutic potential of the drugs solely depends on the actual molecular form of the drugs. The molecular

degradation may produce toxic, undesired and low therapeutically active molecules. The ICH and WHO recommended stress studies as important stability evaluation experiments to determine the molecules' intrinsic stability, shelf life, and degradation mechanism. In-silico degradation profiling helps to predict the type of degradant formed and the underlying degradation mechanism. Numerous studies explain the usefulness of in-silico prediction studies in quantitatively analyzing degradants by analytical methods [33, 34, 41]. The underlying mechanism of LTB and BCA degradation is oxidative hydrolysis. The degradants or impurities associated with BCA and LTB result in skin sensitization and mutagenicity. Thus, it requires compulsion to study each degradant under their force degradations to overcome such toxicity issues related to drug products [34].

The drug nanocarriers are suitable for delivering therapeutic moieties to the disease site. In cancer therapies, NCs have shown prominent results owing to aid in enhanced permeability and retention effect (EPR), improving the bioavailability of poorly aqueous soluble drugs, reducing drug degradation, and offering a suitable environment to load two different types of drugs. The prominent polymeric and lipidic nanocarriers to load two different types of drugs (hydrophilic and hydrophobic) are PLGA NPs and CBs [37, 43]. It finds the developed RP-HPLC method's usefulness in successfully developing the NCs. The selection of appropriate solvent in the development of NCs is crucial as it decides the size of the NCs, polydispersity, % EE, and %DL of the drugs. To access the therapeutic potential of the NCs, the optimum amount of drug must be present inside the drug carrier. Thus, quantification of such is necessary with its mechanism of drug release from NCs. The study depicted the future scopes of studying anti-cancer applications in pre-clinical cancer models.

Conclusion

Combining LTB and a well-known anti-cancer potentiating bioactive, i.e., BCA, may produce effectual anti-cancer therapies in lower doses. An analytical RP-HPLC method for the estimation of LTB and BCA was studied by means of BBD. The method was optimized at mobile phase ratio of ACN: Acidified water pH 4.0 at 85:15, flow rate 0.4 mL/min, injection volume 10 μl to offer peak resolution > 6.5, Tailing < 1.5, and theoretical plates > 5000. The developed method was found to be accurate, precise, specific, robust, and follows all system suitability parameters. The in-silico study helped to predict the actual degradants using RP-HPLC and HRMS studies. LTB and BCA were observed to be degraded in basic hydrolytic and oxidative conditions. The in-silico prediction studies

elaborated on the eighteen and thirty-four degradants for LTB and BCA, respectively. However, the experimental investigation using RP-HPLC and HRMS studies revealed seven LTB degradants and twenty-four BCA degradants. The solubility study of BCA and LTB in a different solvent was studied. The %EE and %DL for LTB and BCA in PLGA NPs and CBs were quantified. The release kinetics study depicted sustained release of BCA and LTB following the First-order release model. However, BCA and LTB release from CBs explained the Higuchi model for release kinetics. The toxicity studies using in-silico prediction software indicate the precautions that need to be taken care of during the development phases for LTB and BCA. Future studies must be encouraged with such chemo-herbal combinations to assess the anti-cancer potential of LTB and BCA. PLGA NPs and CBs can also be explored more for their particle size and shape (scanning electron microscope and transmission electron microscope), solid-state characterization (differential scanning calorimetry and powder X-ray diffraction), in-vitro cell studies, and in-vivo studies.

Abbreviations

% EE	Percentage entrapment efficiency
% DL	Percentage drug loading
ACN	Acetonitrile
AIC	Akaike information criterion
ANOVA	Analysis of variance
BBD	Box–Behnken design
BCA	Biochanin A
CAA	Critical analytical attribute
CBs	Cubosomes
CPP	Critical process parameters
GMO	Glyceryl monooleate
ICH	International Council for Harmonisation
LTB	Lenvatinib
mV	Millivolts
NCs	Nanocarriers
Nm	Nanometer
PDI	Polydisperse index
PLGA NPs	Poly (lactic-*co*-glycolic acid) nanoparticles
QbD	Quality by design
QTMP	Quality-targeted method profile
SD	Standard deviation
USP	United States Pharmacopoeia

Supplementary Information

The online version contains supplementary material available at https://doi.org/10.1186/s43094-023-00561-6.

Additional file 1. The additional file contains the methodology adopted for RP-HPLC method validation. Figures S1, S2, S3, and S4 depict the UV-vis absorption overlay spectrum of LTB and BCA, the validation of quadratic models, the degradation mechanism of LTB, and the degradation mechanism of BCA under different stress conditions, respectively. Tables S1, S2, S3, S4, and S5 explain the ANOVA for quadratic models of responses R1, R2, R3, R4, and R5, respectively. However, table S6 explains the In-silico toxicity data of BCA and LTB using the DEREK software.

Author contributions
AK was involved in the conceptualization, methodology, software, data curation and writing—original draft, SJ assisted in the conceptualization, methodology, and visualization, PK contributed to writing—review and editing, AG was involved in the visualization, supervision, validation, writing—reviewing and editing.

Availability of data and materials
The data that support the findings of this study are available from the corresponding author upon reasonable request.

Declarations

Ethics approval and consent to participate
Not Applicable.

Consent for publication
Not applicable.

Competing interests
The authors declare that they have no known competing financial interests or personal relationships that could have appeared to influence the work reported in this paper.

Author details
[1]Department of Pharmaceutics, National Institute of Pharmaceutical Education and Research Guwahati, Assam 781101, India. [2]Department of Pharmaceutical Analysis, National Institute of Pharmaceutical Education and Research Guwahati, Assam 781101, India.

References

1. Okem A, Henstra C, Lambert M, Hayeshi R (2022) A review of the pharmacodynamic effect of chemo-herbal drug combinations therapy for cancer treatment. Med Drug Discov 17:100147. https://doi.org/10.1016/j.medidd.2022.100147
2. Elgohary M, Helmy M, Abdelfattah E-Z et al (2018) Targeting sialic acid residues on lung cancer cells by inhalable boronic acid-decorated albumin nanocomposites for combined chemo/herbal therapy. J Control Release 285:230–243. https://doi.org/10.1016/j.jconrel.2018.07.014
3. Atallah M, Sallam M, Abdelmoneem M et al (2022) Green self-assembled lactoferrin carboxymethyl cellulose nanogels for synergistic chemo/herbal breast cancer therapy. Colloids Surf B Biointerfaces 217:112657. https://doi.org/10.1016/j.colsurfb.2022.112657
4. Zhu H, Chen H, Zeng X et al (2013) Co-delivery of chemotherapeutic drugs with vitamin E TPGS by porous PLGA nanoparticles for enhanced chemotherapy against multi-drug resistance. Biomaterials 35:2391–2400. https://doi.org/10.1016/j.biomaterials.2013.11.086
5. Zhang S, Zhao L, Peng X et al (2021) Self-assembled phospholipid-based mixed micelles for improving the solubility, bioavailability and anticancer activity of lenvatinib. Colloids Surf B Biointerfaces 201:111644. https://doi.org/10.1016/j.colsurfb.2021.111644
6. Nishio M, Horai T, Horiike A et al (2013) Phase 1 study of lenvatinib combined with carboplatin and paclitaxel in patients with non-small-cell lung cancer. Br J Cancer. https://doi.org/10.1038/bjc.2013.374
7. Makker V, Rasco D, Vogelzang N et al (2019) Lenvatinib plus pembrolizumab in patients with advanced endometrial cancer: an interim analysis of a multicentre, open-label, single-arm, phase 2 trial. Lancet Oncol. https://doi.org/10.1016/S1470-2045(19)30020-8
8. Capozzi M, Divitiis C, Ottaiano A et al (2019) Lenvatinib, a molecule with versatile application: from preclinical evidence to future development in anti-cancer treatment. Cancer Manag Res 11:3847–3860. https://doi.org/10.2147/CMAR.S188316
9. Zhang D, Zhang Y, Cai Z et al (2019) Dexamethasone and lenvatinib inhibit migration and invasion of non-small cell lung cancer by regulating EKR/AKT and VEGF signal pathways. Exp Ther Med. https://doi.org/10.3892/etm.2019.8225
10. Satari N, Taymouri S, Varshosaz J et al (2020) Preparation and evaluation of inhalable dry powder containing glucosamine-conjugated gefitinib SLNs for lung cancer therapy. Drug Dev Ind Pharm 46:1–33. https://doi.org/10.1080/03639045.2020.1788063
11. Xu W, Ye C, Qing X et al (2022) Multi-target tyrosine kinase inhibitor nanoparticle delivery systems for cancer therapy. Mater Today Bio 16:100358. https://doi.org/10.1016/j.mtbio.2022.100358
12. Zhang T, Wang R, Li M et al (2020) Comparative study of intratracheal and oral gefitinib for the treatment of primary lung cancer. Eur J Pharm Sci 149:105352. https://doi.org/10.1016/j.ejps.2020.105352
13. Li J, Xu J, Sun Y et al (2023) An insight on synergistic anti-cancer efficacy of biochanin A and sulforaphane combination against breast cancer. Appl Biochem Biotechnol. https://doi.org/10.1007/s12010-023-04584-w
14. Youssef MM, Tolba MF, Badawy NN et al (2016) Novel combination of sorafenib and biochanin-A synergistically enhances the anti-proliferative and pro-apoptotic effects on hepatocellular carcinoma cells. Sci Rep 6:30717. https://doi.org/10.1038/srep30717
15. Dash TK, Konkimalla VB (2017) Formulation and optimization of doxorubicin and biochanin A combinational liposomes for reversal of chemoresistance. AAPS PharmSciTech 18:1116–1124. https://doi.org/10.1208/s12249-016-0614-z
16. Mahmoud M, Abdollah M, Elsesy M et al (2022) The natural isoflavone Biochanin-A synergizes 5-fluorouracil anticancer activity in vitro and in vivo in Ehrlich solid-phase carcinoma model. Phytotherapy Res. https://doi.org/10.1002/ptr.7388
17. Xiao Y, Gong Q, Wang W et al (2020) The combination of Biochanin A and SB590885 potentiates the inhibition of tumour progression in hepatocellular carcinoma. Cancer Cell Int 20:371. https://doi.org/10.1186/s12935-020-01463-w
18. Sarfraz A, Javeed M, Shah MA et al (2020) Biochanin A: a novel bioactive multifunctional compound from nature. Sci Total Environ. https://doi.org/10.1016/j.scitotenv.2020.137907
19. Jaina V, Eedara A, SVS S et al (2022) Anti-cancer activity of Biochanin A against multiple myeloma by targeting the CD38 and cancer stem-like cells. Process Biochem 123:11–26. https://doi.org/10.1016/j.procbio.2022.10.029
20. Felix F, Vago JP, Beltrami V et al (2022) Biochanin A as a modulator of the inflammatory response: an updated overview and therapeutic potential. Pharmacol Res 180:106246. https://doi.org/10.1016/j.phrs.2022.106246
21. Li Y, Yu H, Han F et al (2018) Biochanin A induces S phase arrest and apoptosis in lung cancer cells. Biomed Res Int. https://doi.org/10.1155/2018/3545376
22. Wang Y, Li JJ, Chen YM (2018) Biochanin A extirpates the epithelial-mesenchymal transition in a human lung cancer. Exp Ther Med 15:2830–2836. https://doi.org/10.3892/etm.2018.5731
23. Manna SK (2012) Double-edged sword effect of biochanin to inhibit nuclear factor kappaB: Suppression of serine/threonine and tyrosine kinases. Biochem Pharmacol 83:1383–1392. https://doi.org/10.1016/j.bcp.2012.02.011
24. Zhang S, Sagawa K, Arnold RD et al (2010) Interactions between the flavonoid biochanin A and P-glycoprotein substrates in rats: In vitro and in vivo. J Pharm Sci 99:430–441. https://doi.org/10.1002/jps.21827
25. Hu X, Qin H, Li Y et al (2020) Biochanin A protect against lipopolysaccharide-induced acute lung injury in mice by regulating TLR4/NF-κB and PPAR-γ pathway. Microb Pathog. https://doi.org/10.1016/j.micpath.2019.103846
26. Shih CH, Ko WC, Lin LH et al (2011) Biochanin A, a phytoestrogenic isoflavone with selective inhibition of phosphodiesterase 4, suppresses ovalbumin-induced airway hyperresponsiveness. Evid Based Complem Altern Med. https://doi.org/10.1155/2011/635058

27. Andugulapati SB, Gourishetti K, Tirunavalli SK et al (2020) Biochanin-A ameliorates pulmonary fibrosis by suppressing the TGF-β mediated EMT, myofibroblasts differentiation and collagen deposition in in vitro and in vivo systems. Phytomedicine. https://doi.org/10.1016/j.phymed.2020.153298

28. Singh SK, Rashid M, Bhalala K et al (2021) A novel nanosized phospholipid complex of Biochanin A for improving oral bioavailability: preparation and in-vitro/in-vivo characterizations. J Drug Deliv Sci Technol. https://doi.org/10.1016/j.jddst.2020.102254

29. Vignaduzzo S, Castellano P, Kaufman T (2008) Method development and validation for the simultaneous determination of meloxicam and pridinol mesylate using RP-HPLC and its application in drug formulations. J Pharm Biomed Anal 46:219–225. https://doi.org/10.1016/j.jpba.2007.09.011

30. Wadhwa G, Krishna K, Dubey S, Taliyan R (2021) Development and validation of RP-HPLC method for quantification of repaglinide in mPEG-PCL polymeric nanoparticles: QbD-driven optimization, force degradation study, and assessment of in vitro release mathematic modeling. Microchem J 168:106491. https://doi.org/10.1016/j.microc.2021.106491

31. Han H-K, Lee B-J, Lee H-K (2011) Enhanced dissolution and bioavailability of biochanin A via the preparation of solid dispersion: In vitro and in vivo evaluation. Int J Pharm 415:89–94. https://doi.org/10.1016/j.ijpharm.2011.05.055

32. Chaudhari V, Borkar R, Murty U, Banerjee S (2020) Analytical method development and validation of reverse-phase high-performance liquid chromatography (RP-HPLC) method for simultaneous quantifications of quercetin and piperine in dual-drug loaded nanostructured lipid carriers. J Pharm Biomed Anal 186:113325. https://doi.org/10.1016/j.jpba.2020.113325

33. Kleinman M, Baertschi S, Alsante K et al (2014) In silico prediction of pharmaceutical degradation pathways: a benchmarking study. Mol Pharm 11:4179–4188. https://doi.org/10.1021/mp5003976

34. Madhyanapu Golla V, Kushwah B, Dhiman V et al (2023) LC-HRMS and NMR studies for characterization of forced degradation impurities of ponatinib, a tyrosine kinase inhibitor, insights into in-silico degradation and toxicity profiles. J Pharm Biomed Anal 227:115280. https://doi.org/10.1016/j.jpba.2023.115280

35. Susanna K, Gajbhiye R, Sarmah B et al (2022) Simultaneous method development and validation of anastrozole along with piperine: degradation studies and degradants characterization using LC-QTOF-ESI-MS along with degradants in-silico ADMET predictions. Curr Drug Metab. https://doi.org/10.2174/1389200223666220215152606

36. Kumar A, Valamla B, Thakor P et al (2022) Development and evaluation of nanocrystals loaded hydrogel for topical application. J Drug Deliv Sci Technol 74:103503. https://doi.org/10.1016/j.jddst.2022.103503

37. Barichello J, Morishita M, Takayama K, Nagai T (1999) Encapsulation of hydrophilic and lipophilic drugs in PLGA nanoparticles by the nanoprecipitation method. Drug Dev Ind Pharm 25:471–476. https://doi.org/10.1081/DDC-100102197

38. Zewail M, Gaafar P, Ali M, Abbas H (2022) Lipidic cubic-phase leflunomide nanoparticles (cubosomes) as a potential tool for breast cancer management. Drug Deliv 29:1663–1674. https://doi.org/10.1080/10717544.2022.2079770

39. Toktas S, Sahin A, Lule S et al (2020) Combination of Paclitaxel and R-flurbiprofen loaded PLGA nanoparticles suppresses glioblastoma growth on systemic administration. Int J Pharm 578:119076. https://doi.org/10.1016/j.ijpharm.2020.119076

40. Inoue K, Asai N, Mizuo H et al (2011) Unique metabolic pathway of [C-14] lenvatinib after oral administration to male cynomolgus monkey. Drug Metab Dispos 40:662–670. https://doi.org/10.1124/dmd.111.043281

41. Dhiman V, Singh S, Balhara A et al (2021) Stress degradation study on entrectinib and characterization of its degradation products using HRMS and NMR. J Pharm Biomed Anal 208:114459. https://doi.org/10.1016/j.jpba.2021.114459

42. Premjeet Singh S, Beg S, Kumar R et al (2017) Analytical Qbd-based systematic bioanalytical HPLC method development for estimation of quercetin dihydrate. J Liq Chromatogr Relat Technol 40:506–516. https://doi.org/10.1080/10826076.2017.1329744

43. Kumar A, Panwar D, Bhavana V et al (2023) Lipid-based nanomaterials: a brief note on composition, development, and drug delivery applications. In: Pardeshi CV (ed) Nanomaterial-based drug delivery systems: therapeutic and theranostic applications. Springer, Cham, pp 65–98

Publisher's Note